GS^{yellow}, a Multifaceted Tag for Functional Protein Analysis in Monocot and Dicot Plants[1][OPEN]

Nienke Besbrugge,[a,b,2] Jelle Van Leene,[a,b,2] Dominique Eeckhout,[a,b] Bernard Cannoot,[a,b] Shubhada R. Kulkarni,[a,b,c] Nancy De Winne,[a,b] Geert Persiau,[a,b] Eveline Van De Slijke,[a,b] Michiel Bontinck,[a,b] Stijn Aesaert,[a] Francis Impens,[d,e,f] Kris Gevaert,[d,e] Daniel Van Damme,[a,b] Mieke Van Lijsebettens,[a,b] Dirk Inzé,[a,b] Klaas Vandepoele,[a,b,c] Hilde Nelissen,[a,b,3] and Geert De Jaeger[a,b,3,4]

[a]Department of Plant Biotechnology and Bioinformatics, Ghent University, 9052 Ghent, Belgium
[b]VIB Center for Plant Systems Biology, 9052 Ghent, Belgium
[c]Bioinformatics Institute Ghent, Ghent University, 9052 Ghent, Belgium
[d]Department of Biochemistry, Ghent University, 9000 Ghent, Belgium
[e]VIB Center for Medical Biotechnology, 9000 Ghent, Belgium
[f]VIB Proteomics Core, 9000 Ghent, Belgium

The ability to tag proteins has boosted the emergence of generic molecular methods for protein functional analysis. Fluorescent protein tags are used to visualize protein localization, and affinity tags enable the mapping of molecular interactions by, for example, tandem affinity purification or chromatin immunoprecipitation. To apply these widely used molecular techniques on a single transgenic plant line, we developed a multifunctional tandem affinity purification tag, named GS^{yellow}, which combines the streptavidin-binding peptide tag with citrine yellow fluorescent protein. We demonstrated the versatility of the GS^{yellow} tag in the dicot Arabidopsis (*Arabidopsis thaliana*) using a set of benchmark proteins. For proof of concept in monocots, we assessed the localization and dynamic interaction profile of the leaf growth regulator ANGUSTIFOLIA3 (AN3), fused to the GS^{yellow} tag, along the growth zone of the maize (*Zea mays*) leaf. To further explore the function of ZmAN3, we mapped its DNA-binding landscape in the growth zone of the maize leaf through chromatin immunoprecipitation sequencing. Comparison with AN3 target genes mapped in the developing maize tassel or in Arabidopsis cell cultures revealed strong conservation of AN3 target genes between different maize tissues and across monocots and dicots, respectively. In conclusion, the GS^{yellow} tag offers a powerful molecular tool for distinct types of protein functional analyses in dicots and monocots. As this approach involves transforming a single construct, it is likely to accelerate both basic and translational plant research.

The field of functional genomics attempts to visualize and describe complex biological processes as molecular interaction networks, using system-wide analysis of gene expression, protein function, and metabolite dynamics (Bunnik and Le Roch, 2013). Since whole-genome sequences have become available, functional genomics has been driven by advancements in omics technologies and bioinformatics. Because proteins are among the key players in these networks, their interactions with other proteins, DNA, RNA, and metabolites are studied extensively.

To circumvent the need for specific antibodies for protein interactome mapping, an affinity tag can be fused to the protein of interest. A variety of affinity tags have been developed, each with specific characteristics and functional applications (Dedecker et al., 2015). Some, like the HA- or FLAG-epitope tags, are applied in coimmunoprecipitation experiments to detect binary interactions among protein pairs. However, by combining affinity purification with mass spectrometry (AP-MS), complexes rather than binary interactions can be identified. Two different AP-MS approaches are generally employed to study protein-protein interactions, using either a single purification step or tandem affinity purification (TAP). The TAP protocol, originally established in yeast (Rigaut et al., 1999), is based on the addition of a dual affinity tag (the TAP tag) to the bait of interest, allowing two subsequent rounds of protein complex purification.

In plants, the TAP-MS protocol has been optimized recurrently, resolving protein complexes from cell cultures (Van Leene et al., 2007), seedlings and whole plants (Rubio et al., 2005; Rohila et al., 2006; Van Leene et al., 2015), and across species such as Arabidopsis

[1]This work was funded by the European Research Council under the European Community's Seventh Framework Programme (FP7/2007-2013) under European Research Council grant agreement [339341-AMAIZE]11 (D.I. and M.B.) and by grants from the Research Foundation-Flanders (G009415N to D.V.D., G001015N to S.R.K., and 1269213N to J.V.L.) and the IWT (121586 to N.B.).

[2]These authors contributed equally to the article.
[3]These authors contributed equally to the article.
[4]Address correspondence to geert.dejaeger@psb.vib-ugent.be.
The author responsible for distribution of materials integral to the findings presented in this article in accordance with the policy described in the Instructions for Authors (www.plantphysiol.org) is: Geert De Jaeger (geert.dejaeger@psb.vib-ugent.be).

G.D.J., N.B., H.N., and J.V.L. designed the research; N.B. carried out the experiments; N.B. and J.V.L. wrote the article; D.E., B.C., N.D.W., E.V.D.S., D.V.D., and G.P. provided technical assistance; S.A. and M.V.L. generated transgenic maize lines; S.K. and K.V. helped with the bioinformatics analysis; D.E., F.I., and K.G. performed MS analyses; J.V.L., H.N., D.I., and G.D.J. supervised and complemented the writing.
[OPEN]Articles can be viewed without a subscription.
www.plantphysiol.org/cgi/doi/10.1104/pp.18.00175

(*Arabidopsis thaliana*), *Medicago truncatula*, maize (*Zea mays*), and rice (*Oryza sativa*; Rubio et al., 2005; Rohila et al., 2006; Nelissen et al., 2015; Goossens et al., 2016). The development of the GS^{rhino} tag, an optimization of the widely used GS TAP tag for mammalian cells (Bürckstümmer et al., 2006), further enhanced the power of the TAP protocol in plants. The GS^{rhino} tag, consisting of two IgG-binding domains of protein G and a streptavidin-binding peptide (SBP), which are separated by two human rhinovirus 3C protease cleavage sites, was shown to outperform other TAP tags in plants, mainly because of its higher specificity (Van Leene et al., 2008, 2015). The emergence of label-free quantification (LFQ) methods for quantitative protein analysis, together with the increased sensitivity of MS detectors, made it possible to use TAP-MS for the determination of protein complex dynamics in a developmental context, as was shown recently for the leaf growth regulator ANGUSTIFOLIA3 in maize (ZmAN3; Nelissen et al., 2015).

In the TAP approach, very pure complexes are obtained with a high signal-to-noise ratio, which is often beneficial for downstream analyses (Van Leene et al., 2008). Moreover, the high specificity of TAP increases the ability to discover substoichiometric complex members, which can get lost among the high background noise when applying single-step purifications. Conversely, single-step purification might be superior for the discovery of low-affinity interactions, which might be lost during the tedious TAP protocol. As a consequence, both approaches reveal complementary subspaces of the protein interactome, and ideally, both should be assessed in parallel to reach the full potential of AP-MS.

Tagging and affinity purification methods also are used intensively in the chromatin immunoprecipitation sequencing (ChIP-seq) method for genome-wide identification of the DNA-binding landscape of transcription factors (TFs) and other DNA-binding proteins. This method starts with the reversible in vivo cross-linking of the bait to its bound DNA regions. Next, chromatin is extracted and fragmented from isolated nuclei, and specific protein-DNA complexes are isolated by a single purification step. Finally, the enriched genomic DNA is released by reverse cross-linking and identified through next generation sequencing.

To minimize the production of transgenic lines for functional protein analysis, multifunctional tags that allow for both visualization of the bait and different immunoprecipitation- or TAP-based interaction studies have been constructed across several species (Paramban et al., 2004; Cheeseman and Desai, 2005; Kobayashi et al., 2008; Schäffer et al., 2010; Ma et al., 2012; De Souza et al., 2014). Since such multifunctional tags have not been implemented in plants, we designed the multifunctional TAP tag GS^{yellow}, which combines elements from the highly efficient GS^{rhino} tag with the fluorescent citrine yellow fluorescent protein (cYFP) tag, broadening its functionality toward visualization of the protein of interest in living cells via microscopy-based techniques. Using a set of well-studied bait proteins involved in growth regulation as a benchmark, the performance of the GS^{yellow} tag for protein visualization, TAP-MS, and ChIP was demonstrated in the dicot Arabidopsis, both in cell cultures and in seedlings. In addition, the GS^{yellow} toolbox was transferred toward the monocot maize, validating subcellular localization patterns and dynamic protein interactions of ZmAN3 along the maize leaf growth zone. Moreover, the GS^{yellow} tag was used for ChIP-seq to identify target genes of ZmAN3 in the maize leaf growth zone, showing a high preference for binding to genes encoding TFs, genes involved in hormone responses and in leaf growth and development, as well as the existence of complex feedback mechanisms. Finally, the ChIP-seq analysis revealed a high degree of conservation of AN3 target genes between different maize tissues and across monocots and dicots. Taken together, this new multifunctional tag provides a generic tool for the functional analysis of proteins and their interaction partners in plants.

RESULTS

A Portfolio of Multifunctional GS^{yellow} Tags

To broaden the functionality of the GS^{rhino} TAP tag in plants (Van Leene et al., 2015), we designed the GS^{yellow} TAP tag, not only to explore protein-protein interactions but also to identify protein-DNA interactions by ChIP-seq and to determine the subcellular localization of the bait protein (Fig. 1). In this TAP tag, the two protein G IgG-binding domains of the GS^{rhino} tag were replaced by cYFP, an improved version of the eYFP that is commonly used as a fluorescent protein in maize (Wu et al., 2013), whereas the SBP and the Gly-4-Ser linker, which bridges the bait protein and the tag, were retained (Supplemental Fig. S1). Besides a shift in the GFP excitation and emission peaks to 514 and 527 nm, respectively, cYFP shows an increase in brightness and resistance against photobleaching, acidic pH, and other environmental factors in comparison with eYFP (Griesbeck et al., 2001), favoring localization analyses in monocots. Given the high protein sequence similarity between GFP and cYFP, the epitopes targeted by anti-GFP antibodies are expected to be conserved. Consequently, the cYFP moiety of the GS^{yellow} tag not only enables anti-GFP-based ChIP analyses or protein complex analysis by anti-GFP immunoprecipitation but, in addition, can be used during the first purification step of an alternative TAP procedure (Fig. 1). Two copies of the tobacco etch virus and the human rhinovirus 3C protease cleavage sites were integrated in the GS^{yellow} tag for soft and flexible elution after the first GFP-based affinity step during TAP. Finally, protein complexes can be further purified at high specificity through the SBP tag in a second streptavidin-based purification step.

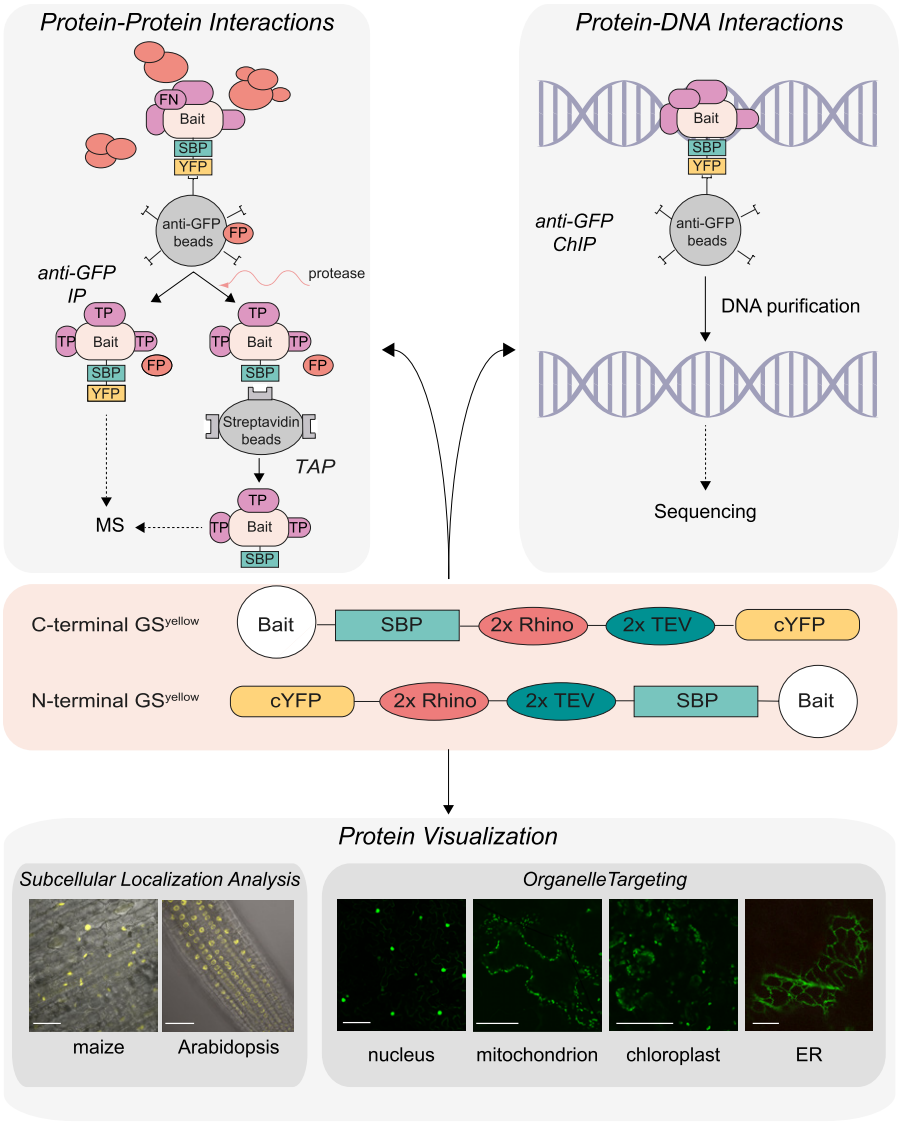

Figure 1. Overview of the multifunctional GS^{yellow} TAP tag molecular toolbox. Both C- and N-terminal fusions of the tag to the bait of interest are shown (middle). The GS^{yellow} tag combines the cYFP with the SBP. Both tags are separated by tandem repeats of tobacco etch virus (TEV) and 3C rhinovirus (Rhino) protease cleavage sites, enabling gentle elution during TAP. The GS^{yellow} tag allows protein complex analysis by AP-MS, either by TAP for highly specific isolation of clean protein complexes or by one-step anti-GFP-based immunoprecipitation (IP; top left). During TAP, complexes are isolated using anti-GFP immunoprecipitation, eluted with TEV or Rhino protease, and further purified using streptavidin beads. FN, False negatives reflecting bona fide interactions lost during AP-MS; FP, false positives isolated based on nonspecific interactions; TP, true positives representing bona fine bait interactions. Purified proteins are identified by MS. For analysis of protein-DNA interactions by ChIP-seq, anti-GFP-based ChIP protocols can be applied on a GS^{yellow} transgenic line (top right). Purified DNA is analyzed by next generation sequencing to identify bound DNA fragments. Finally, the cYFP moiety of the GS^{yellow} tag also enables subcellular localization analysis, both in Arabidopsis and maize (bottom left; bars = 50 μm). For targeting of TAP fusion proteins to specific organelles (bottom right), targeting peptide variants of both the N-terminal GS^{yellow} and GS^{rhino} TAP tags were developed, specifically targeting the nucleus, mitochondria, chloroplasts, or endoplasmic reticulum (ER), as shown by the organelle-targeting peptide variants of the GS^{rhino} tag fused to GFP, transiently expressed in tobacco leaves (bars = 100, 50, 100, and 10 μm, respectively).

Because N-terminal tagging can lead to aberrant subcellular localization of the bait protein by interference with signal peptides present at the native N terminus, an expansion of the GS^{rhino} and GS^{yellow} toolbox for N-terminal tagging was created. Peptides targeting proteins individually to the nucleus (NLS), ER, chloroplasts (Chl), or mitochondria (Mito) were added in front of the N-terminal GS^{rhino} and GS^{yellow} TAP tags. To examine the localization of these peptide sequences, a GFP protein was fused at its N terminus with the

GS^{rhino} targeting peptide TAP tag variants, and subcellular localization was analyzed upon transient expression in tobacco (*Nicotiana tabacum*) leaves. This analysis confirmed the correct localization of all tested organelle-targeting peptide TAP fusions (Fig. 1; Supplemental Fig. S2; NLS_GS^{rhino}-GFP, ER_GS^{rhino}-GFP, Chl_GS^{rhino}-GFP, and Mito_GS^{rhino}-GFP). Although the implemented ER signal encodes the 2S2 apoplast-targeting sequence, it can be used to target proteins to the ER, because apoplastic proteins first pass through the ER. In case the protein has to be retained at the ER, a C-terminal KDEL sequence can be added to the bait protein (Yun and Eipper, 1995).

For efficient and flexible cloning of the GS^{yellow} constructs and the targeting peptide TAP tag variants, multisite Gateway-compatible entry vectors were developed that can be used either for N- or C-terminal cloning to the gene of interest. To evaluate the multifunctionality of the GS^{yellow} tag, Arabidopsis AN3 (Vercruyssen et al., 2014), TPLATE (Van Damme et al., 2006; Gadeyne et al., 2014), and PEAPOD2 (PPD2; Gonzalez et al., 2015) were selected as benchmark bait proteins in Arabidopsis, and ZmAN3 (Nelissen et al., 2015) was selected in maize.

Protein Functionality Is Maintained upon Fusion to GS^{yellow}

Interference of a tag with the full functionality of the bait protein and/or its correct localization is a well-known potential problem associated with protein tagging. An elegant way to test the functionality of the fusion protein is to express the tagged bait protein in the corresponding mutant background and, subsequently, assess complementation of the mutant phenotype. Another way to check for possible interference is overexpression (OE) of the tagged protein in a wild-type background and assessing if the OE phenotype is similar to that of its nontagged counterpart. To address the functionality of GS^{yellow}-tagged proteins and their correct subcellular localization in planta, AN3 and TPLATE were selected for analysis in Arabidopsis. AN3 is a known plant growth regulator that functions as a transcriptional coactivator, linking the SWI/SNF chromatin-remodeling complex to TFs in both Arabidopsis and maize (Vercruyssen et al., 2014; Nelissen et al., 2015). Previous experiments have shown that AN3 localizes to the cell nucleus (Kim and Kende, 2004; Vercruyssen et al., 2014) and that overexpression of *AN3* in Arabidopsis enhances leaf growth as a result of a delay in exit from the mitotic cell cycle, leading to extended cell proliferation before the transition to cell expansion. The function of AN3 in the leaf, however, is broader, because AN3 also is implicated in adaxial/abaxial patterning during leaf morphogenesis (Horiguchi et al., 2011). For functional analysis, AN3 was tagged at the C terminus with the GS^{yellow} tag and expressed from the 35S promoter (p35S) in the wild-type Columbia-0 (Col-0) background. At 21 d after stratification, overexpression of AN3-GS^{yellow} resulted in an increased leaf size and longer petiole phenotype of leaves 3 and 4 compared with wild-type plants (Fig. 2, A and B). This enhanced leaf size agrees with observations following ectopic expression of a nontagged AN3 (Horiguchi et al., 2005; Vercruyssen et al., 2014). In addition to the phenotypes, the reported nuclear localization of AN3 was confirmed in dividing root cells of the AN3-GS^{yellow} line (Fig. 2C). In a previous study, an AN3-GFP fusion protein showed intercellular movement between mesophyll and epidermal cells in Arabidopsis leaves, whereas fusion to the much larger triple GFP fusion prevented this movement (Kawade et al., 2013). Although the movement of AN3-GS^{yellow} across different cell layers was not empirically tested, we expect the GS^{yellow} tag (37 kD) to behave similarly to GFP (27 kD) due to the small difference in molecular mass.

The second benchmark protein that we tested was TPLATE, the founding member of the endocytic TPLATE adaptor complex, which is essential for clathrin-mediated endocytosis at the plasma membrane in plants (Van Damme et al., 2006; Gadeyne et al., 2014). A functional *TPLATE* gene is required for pollen development and the mutation cannot be transferred via the male gametophytes, as it causes fully penetrant male sterility. Reversal of this gametophyte-lethal phenotype can be achieved through the expression of *TPLATE* from a pollen-specific promoter, pLat52 (Van Damme et al., 2006). To investigate the functionality of TPLATE fused to the GS^{yellow} tag, we transformed a construct expressing *TPLATE* from the Lat52 promoter, tagged at its C terminus with the GS^{yellow} tag, into a heterozygous *TPLATE* mutant background. A transgenic line heterozygous for the *TPLATE* mutation and homozygous for the transgene was isolated. After selfing of this line, complementation of the *TPLATE* mutation by the TPLATE-GS^{yellow} fusion protein was confirmed through a segregation analysis, in which the progeny ratios shifted from the typical gametophyte-lethal 1:1 ratio in the heterozygous *TPLATE* mutant to a normal Mendelian inheritance pattern of 1:2:1 in the complemented plant line (Fig. 2D). Scanning electron microscopy analysis of the pollen grains obtained from this complemented line confirmed full complementation, as demonstrated by the complete restoration of pollen viability (Fig. 2E). In addition to the pollen-specific expression pattern in flowers, combining the pLat52 promoter with the TPLATE open reading frame leads to basal transcriptional activity in somatic tissues of Arabidopsis seedlings (Van Damme et al., 2006). This extended expression pattern permitted us to study the dynamic subcellular localization of TPLATE-GS^{yellow} in the hypocotyls using spinning disc confocal microscopy. In agreement with the results obtained with pLat52:TPLATE-GFP in the homozygous *tplate* mutant (Gadeyne et al., 2014), we show dynamic recruitment of the TPLATE-GS^{yellow} fusion protein at the plasma membrane with an average dwell time of 20 s (n = 964; Fig. 2F). The above results clearly show that the GS^{yellow} tag can be used for localization analysis and that

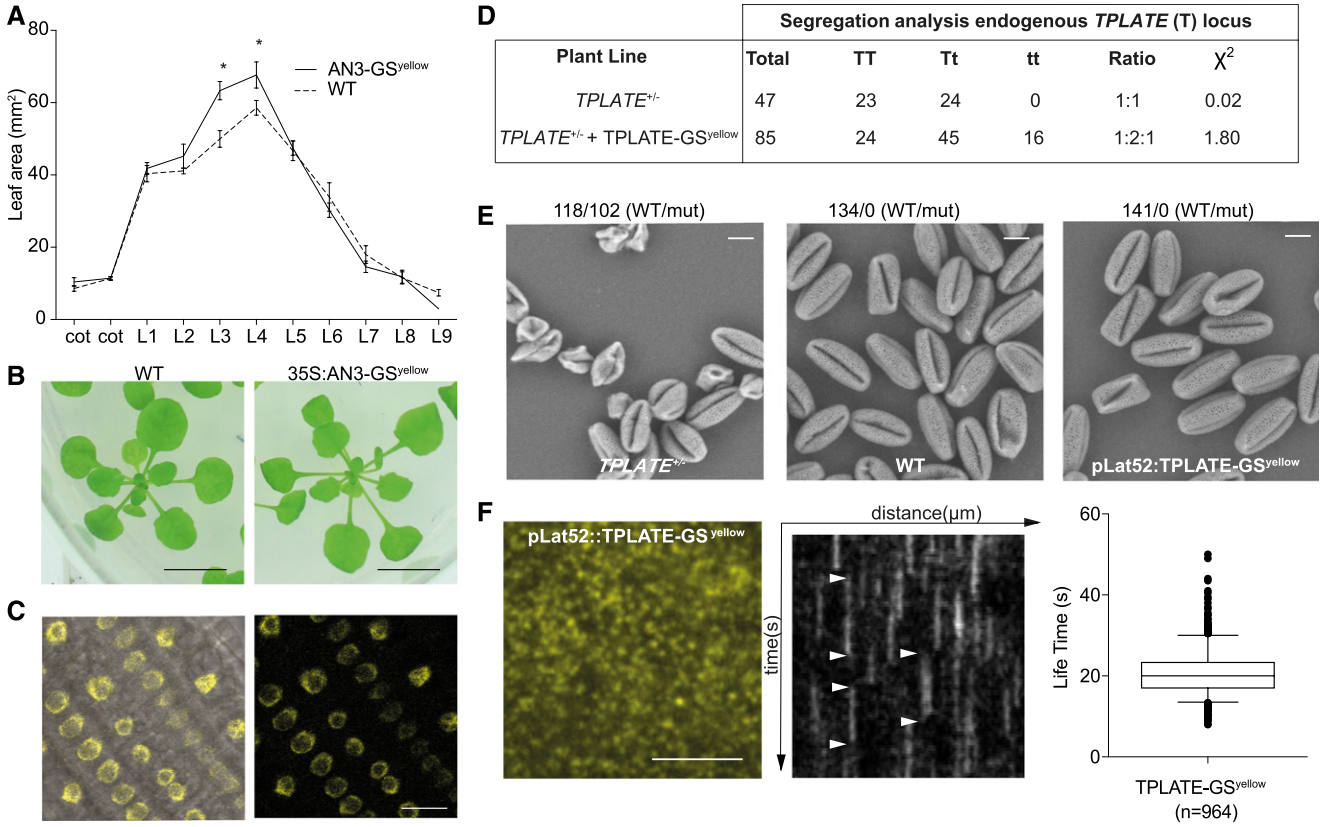

Figure 2. Functional analysis of GS^{yellow}-tagged AN3 and TPLATE. A, Leaf areas of 21-d-old wild-type (WT) or AN3-GS^{yellow}-overexpressing plants grown on control medium. The areas of cotyledons (cot) and leaves 1 to 9 (L1–L9) were measured from leaf series. Error bars represent SE ($n = 3$), and asterisks indicate significant differences from the wild type (Col-0; $P < 0.05$, Student's *t* test). B, Representative rosettes of 21-d-old plants used for leaf series. Bars = 1 cm. C, Confocal microscopy images of the root tip from a 6-d-old seedling expressing 35S:AN3-GS^{yellow}, showing nuclear localization of AN3. Bar = 20 µm. D, Segregation analysis of the endogenous *TPLATE* locus in the offspring produced by selfing the heterozygous *TPLATE* mutant or the heterozygous *TPLATE* mutant complemented homozygously with pLat52:TPLATE-GS^{yellow}. TT = *TPLATE* +/+, Tt = *TPLATE* +/−, tt = *TPLATE* −/−. χ^2 values for the observed segregation ratios are indicated. The observed values do not differ significantly from the expected values for the indicated ratios ($\chi^2 = 3.84$ at $P < 0.05$). E, Scanning electron microscopy images of pollen grains derived from heterozygous *TPLATE* mutant plants, wild-type plants, and a complemented mutant heterozygous for the *TPLATE* mutation and homozygous for pLat52:TPLATE-GS^{yellow}. Ratios of wild-type versus mutant (mut) pollen are indicated. Bars = 10 µm. F, Left, Representative spinning disc confocal microscope image of a hypocotyl epidermal cell belonging to a *TPLATE* mutant plant complemented with pLat52:TPLATE-GS^{yellow}, taken from the corresponding movies. Bar = 5 µm. Middle, Discrete, dynamic foci represent the recruitment of TPLATE, which can be measured over time through a kymograph (arrowheads indicate the beginning and end of the signal). Right, TPLATE-GS^{yellow} has an average dwell time of 20 s at the plasma membrane ($n = 964$).

fusion to the tag does not interfere with the functions of AN3 or TPLATE.

The GS^{yellow} Tag Performs Equally Efficiently as the GS^{rhino} Tag for the Isolation of Protein Complexes through TAP in Arabidopsis

Next, we examined the performance of the multifunctional GS^{yellow} tag for the identification of protein interaction partners through TAP by comparison with the GS^{rhino} TAP tag. AN3, TPLATE, and PPD2 were selected as benchmark bait proteins for comparative TAP in cell cultures. In addition, AN3 and TPLATE were selected for TAP in seedlings because of prior knowledge of their complex composition in seedlings (Gadeyne et al., 2014; Vercruyssen et al., 2014). Transgenic cell cultures with both GS^{rhino}- and GS^{yellow}-tagged versions of each bait protein were generated in parallel. Duplicate TAP experiments were performed using equal total protein inputs for each GS^{yellow}-GS^{rhino} bait pair, and purified proteins were detected by MS (Supplemental Table S1A). To correct for false-positive interactors, a list of 936 nonspecific proteins (Supplemental Table S1B) was used to filter the proteins detected by MS. This list represents an updated list of nonspecific proteins determined as described previously (Van Leene et al., 2015), now covering 803 TAP experiments in cell culture or seedlings, among 163 bait proteins tagged with the GS, GS^{rhino}, or GS^{yellow} tag. After removal of these false positives, a list of specific

Table I. Evaluation of GS^{yellow} performance for TAP in Arabidopsis by comparison with the GS^{rhino} TAP tag and with previously reported TAP results of AN3 (Vercruyssen et al., 2014), TPLATE (Gadeyne et al., 2014), and PPD2 (Gonzalez et al., 2015)

Constructs in cell cultures were expressed through the constitutive 35S promotor. For in planta TAPs (seedlings), pLat52:TPLATE-GS^{yellow} was transformed into the heterozygous *TPLATE* mutant, whereas 35S:AN3-GS^{yellow} was transformed in wild-type Col-0. All TAPs were performed as two technical repeats, except for the TPLATE seedlings TAPs, which represent biological repeats. The numbers indicate how often a protein was detected over the two repeat experiments. Only specific interactors were retained. The SWI/SNF core subunits in the AN3 TAPs are indicated with asterisks. PPD2 seedling TAPs were not tested (NT).

Bait	Protein Identifier	Protein Name	Cell Cultures		Seedlings	Previously Reported
			GS^{yellow}	GS^{rhino}	GS^{yellow}	
AN3	AT5G28640	AN3	2	2	2	x
	AT1G18450	ARP4*	2	1	2	x
	AT3G60830	ARP7*	2		2	x
	AT4G22320	BCL7B-1*			1	x
	AT5G55210	BCL7B-2*	2		2	x
	AT1G20670	BRD1*	2		2	x
	AT5G55040	BRD13*	2		1	x
	AT1G76380	BRD2*	2			x
	AT2G46020	BRM*	2	2	2	x
	AT4G18480	CHLI1			2	
	AT5G07940	Dentin sialophosphoprotein	2		2	x
	AT5G07980	Dentin sialophosphoprotein	2			x
	AT4G17330	G2484-1*	2	2	2	x
	AT5G17510	GLTSCR*	2		2	x
	AT2G36400	GRF3			1	x
	AT3G22990	LFR*			2	x
	AT1G21700	SWI3C*	2	1	2	x
	AT4G34430	SWI3D*	2	1	2	x
	AT3G01890	SWP73A*			2	x
	AT5G14170	SWP73B*	2	1	2	x
	AT2G28290	SYD*	2	2	2	x
	AT4G35550	WOX13	1	1	2	x
TPLATE	AT3G01780	TPLATE	2	2	2	x
	AT3G50590	TWD40-1	2	2	2	x
	AT5G24710	TWD40-2	2	2	2	x
	AT5G57460	TML	2	2	2	x
	AT2G07360	TASH3	2	2	2	x
	AT1G20760	AtEH1	2	2	2	x
	AT1G21630	AtEH2	2	2	2	x
	AT1G15370	LOLITA	2	1	2	x
PPD2	AT4G14720	PPD2	2	2	NT	x
	AT4G28910	NINJA	2	2	NT	x
	AT4G32295	KIX8	2	2	NT	x
	AT3G17860	JAZ3	2	2	NT	x
	AT4G32570	TIFY8	2	1	NT	x
	AT3G24150	KIX9	1		NT	x

interactors found per tag was obtained for each bait protein (Table I).

Previously, TAP experiments revealed conservation of the interaction of AN3 with the SWI/SNF chromatin-remodeling complex in Arabidopsis and maize (Vercruyssen et al., 2014; Nelissen et al., 2015). Moreover, multiple interactions were identified with TFs such as with growth regulatory factors (GRFs) and with WUSCHEL-related homeobox13 (WOX13; Nelissen et al., 2015). TAP on AN3-GS^{yellow} Arabidopsis cell cultures detected 13 subunits of the SWI/SNF chromatin-remodeling complex (Table I), together with three additional proteins (WOX13 and two dentin sialophosphoprotein-related proteins, AT5G07940 and AT5G07980), which are thought to associate either with the core SWI/SNF complex or with AN3 (Vercruyssen et al., 2014; Nelissen et al., 2015). For the GS^{rhino}-tagged version of AN3, only seven SWI/SNF core subunits were retrieved, together with WOX13. When the TAPs with AN3-GS^{yellow} were performed on seedling extracts, 15 out of the 16 reported interacting proteins found with TAP in planta were confirmed (Table I; Supplemental Table S1C; Vercruyssen et al., 2014). In contrast to the previous seedling TAPs, two additional core SWI/SNF complex subunits were identified, BCL7B-1 and dentin sialophosphoprotein-related AT5G07940 (Nelissen et al., 2015; Sarnowska et al., 2016). Besides these 17 core proteins, the seedling experiments also confirmed the association with WOX13 as well as the interaction with GRF3 (Debernardi et al., 2014), although the latter was found only once over the two TAP duplicates (Table I).

To further assess the functionality of the GS^{yellow} tag for TAP-MS in cell culture and seedlings, we analyzed TPLATE interactors, as the endocytosis-related TPLATE complex has been reported to consist of eight subunits (Gadeyne et al., 2014). For the TPLATE cell culture TAPs, both the GS^{yellow} and GS^{rhino} TAPs purified the complete octameric complex (Table I). Subsequent TAPs on seedlings of the complemented pLat52:TPLATE-GS^{yellow} transgenic line confirmed the capacity of the GS^{yellow} tag to identify all components of the octameric TPLATE complex from plants (Table I).

Finally, the performance of the GS^{yellow} tag in TAP was analyzed on PPD2, a class II TIFY protein (Cuéllar Pérez et al., 2014) that regulates leaf development through the repression of asymmetric meristemoid division (Gonzalez et al., 2015). Cell culture TAP analyses have shown that PPD2 interacts with other proteins belonging to TIFY class II, with NINJA, and with members of the KIX protein family (Gonzalez et al., 2015). In our analysis, NINJA and two class II TIFY proteins (jasmonate-zim-domain protein3 and TIFY8) were validated as PPD2 interactors using both TAP-tagged versions of the bait (Table I). Moreover, interactions with the KIX protein family members KIX8 and KIX9 were confirmed with the GS^{yellow} tag, whereas the GS^{rhino} tag only copurified KIX8.

Given the high overlap of the GS^{yellow} interaction data for three independent bait proteins with previously published data and with the new GS^{rhino} TAP results, it is clear that the performance of the GS^{yellow} tag is comparable to that of the GS^{rhino} tag, enabling protein complex analysis in both Arabidopsis cell cultures and seedlings.

Extension of the GS^{yellow} Tag for ChIP-seq Analysis in Arabidopsis

Besides implementing the GS^{yellow} TAP tag for the discovery of protein-protein interactions, its performance was evaluated for the identification of protein-DNA interactions through ChIP-seq in Arabidopsis. For proof of concept, the genome-wide DNA-binding landscape of the PPD2 repressor was analyzed by ChIP-seq in cell culture. In the benchmark study (Gonzalez et al., 2015), genes bound by PPD2 were identified by tandem chromatin affinity purification (TChAP)-seq analysis (Verkest et al., 2014) on a PPD2-His-Bio-His (HBH) transgenic cell culture. This analysis showed that PPD2 mainly targets promoter regions, which were enriched with a G-box motif (CACGTG) as a cis-regulatory element. Gene Ontology (GO) enrichment analysis showed a preference for binding genes involved in transcriptional regulation and in hormone metabolism. Integration of the TChAP-seq data with transcriptome data from Arabidopsis *ppd2* knockdown plants revealed a set of 13 repressed direct target genes, including two D3-type cyclins, providing insight into how PPD2 restricts meristemoid division. In the PPD2 benchmark study (Gonzalez et al., 2015), the GS^{yellow} tag was used for ChIP-quantitative PCR confirmation of five PPD2 direct target genes (*CYCD3;2*, *CYCD3;3*, *ALCATRAZ*, *SCHLAFMUTZE*, and *PPD2*). For this ChIP-quantitative PCR confirmation analysis, an existing GFP-based ChIP protocol (Morohashi et al., 2012) was adapted for ChIP with the GS^{yellow} tag.

To obtain a more comprehensive view of the performance of the GS^{yellow} tag in ChIP, we performed a genome-wide ChIP-seq analysis on PPD2-GS^{yellow} cell cultures and compared this with the PPD2-HBH TChAP-seq results. To increase the stringency of the obtained data, two technical ChIP-seq repeats were performed. For normalization, a negative control ChIP-seq was done on a nucleus-localized version of the GS^{yellow} tag (NLS-GS^{yellow}). After read mapping and peak calling, the identified targets were compared with data derived from two PPD2-HBH TChAP-seq experiments, which were normalized to a mock wild-type TChAP control. Because the previously reported data set of the first PPD2-HBH TChAP-seq analysis (Gonzalez et al., 2015) was created using an older version of the peak calling tool MACS, it was here reanalyzed along with a new PPD2-HBH TChAP-seq experiment. Upon merging the output of the two HBH TChAP experiments, 1,096 peaks corresponding to 1,034 genes were identified in the intersection of both experiments, retaining 11 of the 13 previously reported transcriptionally regulated direct target genes (Supplemental Table S2A).

For PPD2-GS^{yellow}, 1,562 peaks corresponding to 1,336 genes were found in the intersection between the two replicates (Supplemental Table S2B). Comparison of the GS^{yellow} and HBH results showed that 45% of the PPD2-HBH target genes were confirmed by PPD2-GS^{yellow} (Fig. 3A). Of the 11 transcriptionally regulated target genes found in both HBH TChAP replicates (see above), 10 were confirmed in both GS^{yellow} replicates. When zooming in at the peak level, nine peaks covering eight of the transcriptionally regulated targets showed a similar peak localization pattern in both the HBH and GS^{yellow} data sets (Table II; Supplemental Table S2C). Although the TChAP-seq experiments validated one additional transcriptionally regulated direct target, these targets were ranked higher in order in the GS^{yellow} data set when the lists were sorted according to their fold enrichment (Table II). For the GS^{yellow} ChIPs, four out of the eight transcriptionally regulated direct targets were present among the 100 most enriched genes, compared with only one for the HBH tag, indicating more specific enrichment of true regulated targets with the GS^{yellow} tag. In addition, a significant overlap was found for both the GS^{yellow} (13.4%, P = 3.02E-10) and HBH (14%, P = 7.43E-10) data sets when compared with genes recently reported to be differentially expressed in a *ppd* deletion mutant (White, 2017).

Analysis of the localization of the mapped peaks retained by each tag demonstrated that most binding events occurred in the 5′ untranslated region and the 1-kb upstream region (Fig. 3, A–C), validating the binding of PPD2 to gene promoter regions. Furthermore, a de novo motif analysis identified overrepresentation of

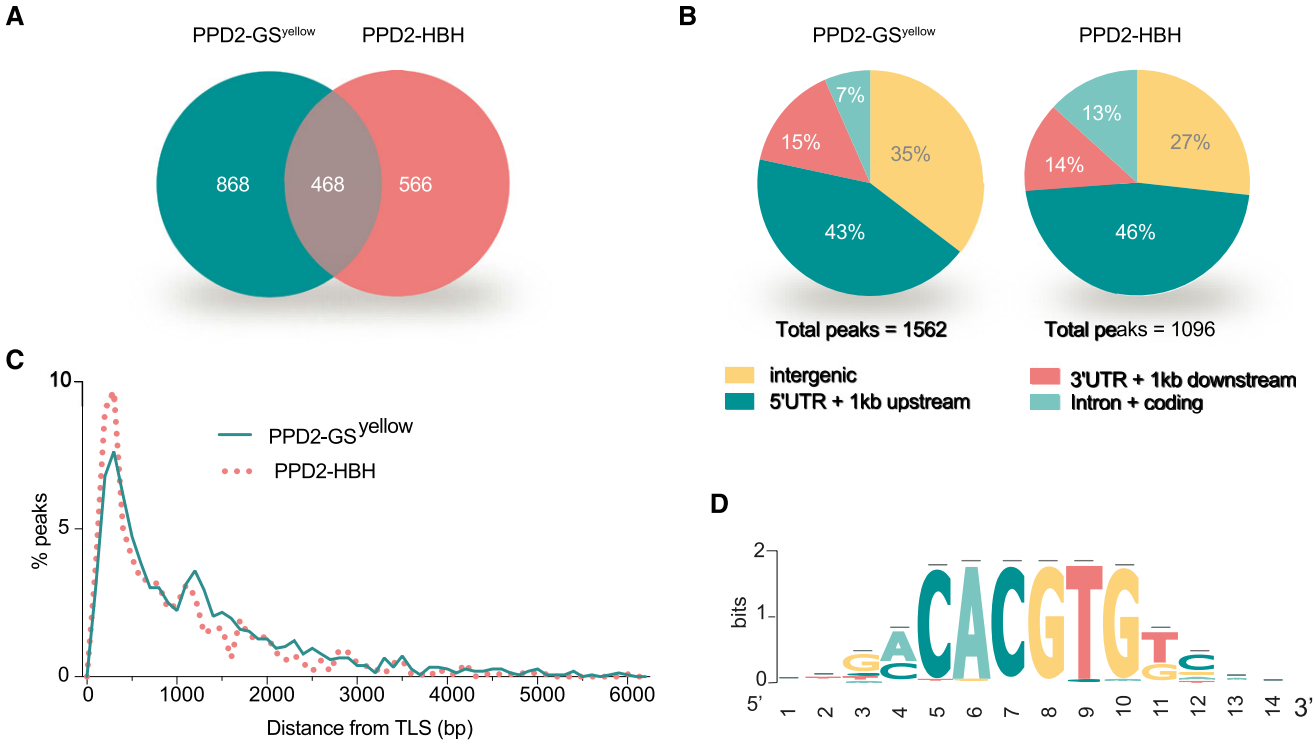

Figure 3. Genome-wide ChIP-seq analysis of PPD2-GS^{yellow}. ChIP was performed with an anti-GFP antibody on cell suspension cultures (PSB-D) transformed with 35S:PPD2-GS^{yellow}. The data were normalized to a 35S:NLS-GS^{yellow}-expressing PSB-D culture and compared with TChAP on PSB-D cultures transformed with 35S:PPD2-HBH (Gonzalez et al., 2015). A, Venn diagram of genes shared in each retrieved gene list after normalization. B, Genome-wide distribution of PPD2 DNA-binding sites in relation to the gene structure. Only peaks present in the intersects of both replicates were considered. UTR, Untranslated region. C, Distribution of the distance of peak summits to the nearest annotated translation start site (TLS) in bp. D, Graphic representation of the enriched G-box motif bound by PPD2, as determined through de novo motif analysis on the GS^{yellow} ChIP data.

the reported G-box in both PPD2-GS^{yellow} samples (Fig. 3D). A GO enrichment analysis of the GS^{yellow} data set confirmed the TChAP data, showing that PPD2 has a preference for binding to genes involved in transcriptional regulation ($P < 1.38E-30$) and hormone response ($P < 2.86E-34$; Supplemental Table S3, A and B). Interestingly, when we analyzed the 250 most strongly enriched genes of the subsets that were unique for either the GS^{yellow} or the HBH tag intersects, these two GO terms were much more significantly enriched with the GS^{yellow} tag (Supplemental Table S3, C and D). In the end, by combining the PPD2-GS^{yellow} and PPD2-HBH data sets, a stringent data set covering 468 genes was obtained (Supplemental Table S2C), offering a reliable

Table II. Overview of genes transcriptionally regulated by PPD2 that are present in both the PPD2-GS^{yellow} and PPD2-HBH ChIP intersects

Published direct target genes of PPD2 (Gonzalez et al., 2015) are shown, together with their fold enrichments (FE) and significance [–Log(q)] in both the PPD2-GS^{yellow} and PPD2-HBH intersects. Boldface numbers indicate ranking of the FE value in the top 100 of highest enriched targets. Ranking is based on the first replicate.

Closest Gene	Gene Symbol	PPD2-GS^{yellow}			PPD2-HBH		
		Rank	FE	–Log(q)	Rank	FE	–Log(q)
AT5G67260	CYCD3;2	**32**	7.56	49.40	149	6.27	37.22
AT3G50070	CYCD3;3	**47**	7.02	43.29	179	5.57	31.47
AT3G54990	SMZ	**79**	6.28	35.01	252	4.81	26.55
AT2G37630	AS1	**92**	6.08	32.62	154	6.18	29.08
AT5G67110	ALC	109	5.87	31.06	114	6.84	38.20
AT5G54510	DFL	197	5.13	23.60	**20**	11.87	97.01
AT1G14900	HMGA	262	4.82	37.74	511	3.61	24.06
AT1G23870	TPS9	466	4.26	32.38	1055	2.05	7.07
AT5G54510	DFL	645	3.78	19.45	570	3.41	12.76

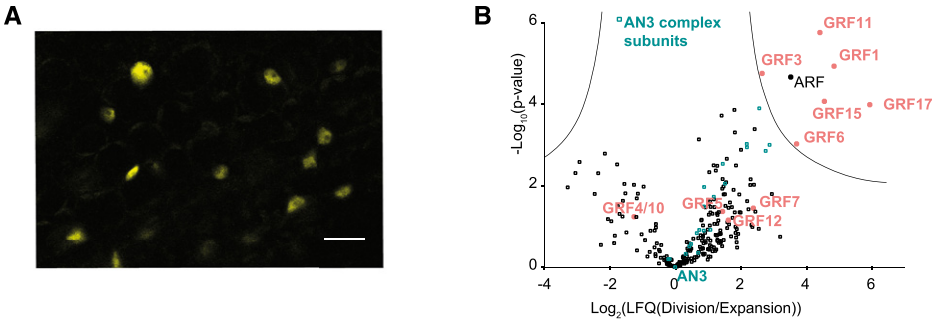

Figure 4. Functional analysis of ZmAN3-GS^{yellow} along the maize leaf growth zone. A, Confocal microscopy image of the division zone of leaf 4 at 2 d after emerging, showing nuclear localization of ZmAN3. Bar = 20 µm. B, Relative intensity-based label-free quantification of copurified proteins identified with TAP on ZmAN3-GS^{yellow} shown in a volcano plot. Comparison between the division zone and the expansion zone delineates significant changes of interaction partners between the zones. GRFs and AN3 core complex members are indicated in red and blue, respectively.

source to the community for further functional analysis of PPD2. Taken together, these data show that the multifunctional GS^{yellow} tag can be used for ChIP analysis in Arabidopsis applying a standard GFP-based ChIP protocol.

Dynamic Protein-Protein Interaction Mapping in Maize with the GS^{yellow} Tag

To assess the performance of the GS^{yellow} tag in other plant species, the multifunctionality of the tag was tested in the monocot maize. The leaf growth regulator ZmAN3, which is the ortholog of Arabidopsis AN3 (Nelissen et al., 2015), was selected as the benchmark protein. The maize leaf is an excellent system in which to investigate leaf development because of its linear organization, spatially separating the leaf growth zone into zones of cell division and cell expansion. Previously, the dynamics of the ZmAN3 protein complex along the different growth zones of the maize leaf were mapped by GS TAP experiments (Nelissen et al., 2015), revealing the stable interaction of ZmAN3 with the SWI/SNF complex along the leaf growth zone, whereas dynamic interactions were observed with GRFs (Nelissen et al., 2015). Using these results as a benchmark, the performance of the multifunctional GS^{yellow} tag in maize was assessed by fusion of the tag to the C-terminal end of ZmAN3. A transgenic maize line, called ZmAN3-GS^{yellow}, was generated containing a single T-DNA locus. Similar to the benchmark maize study, expression was driven by a mild constitutive ubiquitin promoter (pUBIL; Coussens et al., 2012), enhancing the competition for interaction partners with the endogenous ZmAN3. After detection of the transgene-derived fusion protein by western blotting, this ZmAN3-GS^{yellow} line was used for all further analyses. In agreement with the previous study where the pUBIL:ZmAN3-GS line was analyzed (Nelissen et al., 2015), the overall final leaf size of the resulting pUBIL:ZmAN3-GS^{yellow} line was not significantly different from that of the nontransgenic siblings (Student's *t* test, $P = 0.24$; $n \geq 15$; Supplemental Fig. S3), but the pUBIL:ZmAN3-GS^{yellow} plants developed slower than the nontransgenic siblings. The lack of a growth phenotype is in contrast to the phenotype observed in Arabidopsis, where overexpression of AN3 leads to an increase in final leaf size (Vercruyssen et al., 2014). In Arabidopsis, however, the strong 35S promoter was used, whereas in maize, we used the milder ubiquitin promoter. One possible explanation for this discrepancy is that the strength of the phenotypes correlates with the overexpression levels obtained in leaves. To confirm that the GS^{yellow} fusion protein was functional, its localization pattern was examined at the subcellular level. Confocal microscopy analysis of the basal part of leaf 4, reflecting the division zone, showed accumulation of the YFP signal in the nucleus (Fig. 4A), in agreement with the localization pattern observed in Arabidopsis (Vercruyssen et al., 2014).

For dynamic protein interactome mapping with the GS^{yellow} tag along the maize leaf growth zone, separate protein extracts were prepared from either the division or expansion zone of the emerging leaf 4, and five TAP experiments were performed for each zone. After MS-based identification of copurifying proteins (Supplemental Table S4A), background and nonspecific proteins (Supplemental Table S4, B and C) were filtered out. The resulting ZmAN3-GS^{yellow} TAP network (Table III) mainly reiterated known ZmAN3 interactions, next to some additional copurified proteins (Supplemental Table S4D). Comparison with the known GS TAP network shows that we were able to copurify the complete SWI/SNF core complex in both growth zones, even further expanding the complex with additional homologs for several complex members (BCL7, BRD1, and SWI3D). Also, the interaction pattern of the GRF family in the leaf growth zone was in agreement with the GS TAP network. Interestingly, GRF11, previously identified as a ZmAN3 interactor that is specific for the ear, was now also found in the leaf. To further analyze the dynamic nature of the GRF interactors in more detail, the label-free quantitative MS data were

Table III. Evaluation of GS^{yellow} performance in TAP experiments on ZmAN3 in maize

The data were compared with previously published results in maize (Nelissen et al., 2015). The numbers of experiments are indicated in parentheses.

Protein Identifier	Protein Name	GS^{yellow}		Previously Reported	
		Division Zone (5)	Expansion Zone (5)	Division Zone (4)	Expansion Zone (4)
Core subunits					
GRMZM2G180246	ZmAN3	5	5	4	4
GRMZM2G015384	ARP4	5	5	4	4
GRMZM2G015861	ARP7	5	5	4	4
GRMZM2G018955	BCL7	5	5	4	2
GRMZM2G005646	BCL7	5	5		
GRMZM2G020548	BRD1	5	5	4	2
GRMZM2G044044	BRD1	5	5	2	1
GRMZM2G336962	BRD1	5	3		
GRMZM2G353779/ GRMZM2G312501	BRD1	5	5	3	3
GRMZM2G163849	BRM	5	5	4	4
GRMZM2G103079	Dentin sialophosphoprotein	5	5	4	4
GRMZM5G816791	Dentin sialophosphoprotein	5	5	4	4
GRMZM2G473310	G2484-1	5	5	4	4
GRMZM2G033478	G2484-1	5	5	4	4
AC198518.3_ FGP003	GLTSCR	5	5	4	4
GRMZM2G476652	LFR	5	5	3	3
GRMZM2G139760	SWI3C (SWIRM)	5	5	4	2
GRMZM2G340756	SWI3C (SWIRM)	5	5	4	4
GRMZM2G119261	SWI3D (CHB3)	5	4		
GRMZM2G047038	SWI3D (CHB3)	5	5	4	4
GRMZM2G052416	SWP73B (CHC1)	5	5	4	4
GRMZM2G467799	SYD	5	5	4	4
GRMZM2G387890	SYD	5	5	4	4
GRFs					
GRMZM2G034876	GRF1	5	3	4	2
GRMZM2G096709/ GRMZM2G004619	GRF4/GRF10	4	5	4	4
GRMZM2G067743	GRF11	5	4		
GRMZM2G119359	GRF12	5	4	4[a]	
GRMZM2G178261	GRF15	5[a]		4	
GRMZM2G124566	GRF17	5	1	4	1
GRMZM2G105335	GRF3	5[a]		2	
GRMZM2G129147	GRF5	5	1	2	
GRMZM2G041223	GRF6	5	1	3	
GRMZM5G850129	GRF7	5	4	4	

[a]Identified with one significant peptide.

statistically compared over the two growth zones. This analysis identified seven interactors that were enriched significantly in the division zone, including six GRFs and an auxin response factor, while the bait and the core SWI/SNF subunits were stable between the two zones (Fig. 4B; Supplemental Table S4E). The division zone-specific GRFs show a high overlap with the ones reported previously (Nelissen et al., 2015), confirming four dynamic GRFs (GRF1, GRF6, GRF15, and GRF17). Moreover, although both proteins could not be discriminated on the MS level, the quantitative analysis validated that GRF4 and/or GRF10, which are both insensitive to the microRNA *miR396b* that targets *GRF* transcripts, interact(s) with ZmAN3 in both the division as well as the expansion zone. Taken together, these data show that the GS^{yellow} TAP tag can be used to isolate and map dynamic protein complexes in the maize leaf.

Identification of ZmAN3 Target Genes through GS^{yellow}-Based ChIP-seq in Maize

Finally, we assessed whether a GFP-based ChIP protocol using GS^{yellow} also can be applied to maize. Here, genome-wide target genes of ZmAN3-GS^{yellow} were identified through ChIP-seq on the growth zone of the maize leaf. As benchmarks, two different studies were used. In the first study, ZmAN3 target genes were identified in developing tassels of maize through a comparison of genes differentially expressed in a *ZmAN3* mutant with genes bound by ZmAN3-GFP (Zhang et al., 2018), whereas in the second study, Arabidopsis

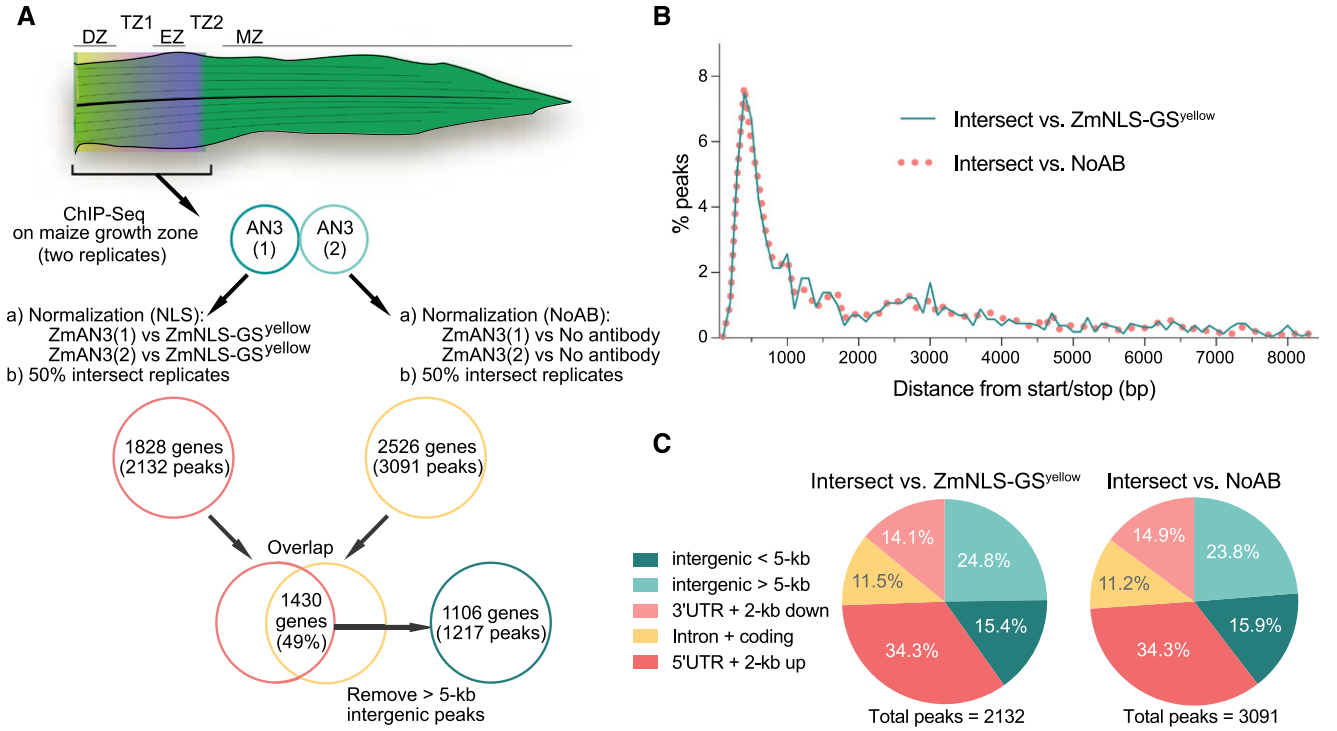

Figure 5. Identification of genome-wide ZmAN3-GS^{yellow} binding sites through ChIP-seq on the growth zone of leaf 4 in maize. ChIP experiments were carried out in parallel on the full growth zone (cm 1–4) of leaf 4 at 2 d after emerging. A, Overview of the strategy used to identify genome-wide target genes of ZmAN3 through ChIP-seq. Normalization against two negative controls (NoAB and ZmNLS-GS^{yellow}) was carried out on two ZmAN3 replicates. For each normalization method, peaks in common between the two replicates were identified if 50% or more of the peaks overlapped. To identify high-confidence peaks, only peaks were retained in the overlap of both normalization methods, and peaks locating in greater than 5-kb intergenic regions were removed. B, Distance distribution per negative control in bp of ZmAN3 peak summits to the closest translation start or stop site. C, Schematic representation of genome-wide ZmAN3-binding sites in relation to the gene structure. UTR, Untranslated region.

AN3 target genes were mapped by HBH-based TChAP-seq experiments in Arabidopsis cell culture (Vercruyssen et al., 2014). For the ZmAN3-GS^{yellow} experiments in maize, two replicate ChIP samples were generated from the growth zone encompassing the division, transition, and expansion zones of the ZmAN3-GS^{yellow} transgenic line (Fig. 5A). Each replicate was normalized against two different negative controls: (1) extracts derived from a maize transgenic line expressing a nucleus-localized version of the GS^{yellow} tag (pUBIL:ZmNLS-GS^{yellow}), and (2) a no-antibody control (NoAB) on extracts derived from ZmAN3-GS^{yellow}, in which the anti-GFP antibody used during ChIP to enrich the AN3-GS^{yellow}-bound chromatin fragments was omitted. To increase the stringency of the obtained data, only peaks found in common (peak intersect, 50% or greater) between both ZmAN3-GS^{yellow} replicates were considered. Normalization against the ZmNLS-GS^{yellow} control rendered 2,132 common peaks mapping to 1,828 genes (Supplemental Table S5A), whereas with normalization against the NoAB control, 3,091 common peaks mapping to 2,526 genes were identified (Fig. 5A; Supplemental Table S5B). Both normalization methods generated a similar peak distribution, covering mainly binding events located in close proximity of genes (Fig. 5B). Although the binding of ZmAN3 was located in a variety of genomic contexts, the highest fraction of peak summits was found in the 2-kb upstream region, reflecting binding events mainly in promoter regions (Fig. 5C). This preference for binding in promoter regions is in agreement with the maize and Arabidopsis ChIP-seq data and corroborates the molecular function of AN3 as a coactivator of gene expression (Vercruyssen et al., 2014; Zhang et al., 2018). To further increase the stringency of the obtained data, two additional filters were applied (Fig. 5A). First, only peaks found in the overlap of both normalization methods were taken into account (Supplemental Table S5C). Second, in agreement with a previous maize ChIP study (Morohashi et al., 2012), peaks were removed that were located in intergenic regions more than 5 kb upstream of the translation start or 5 kb downstream of the translation stop. These filtering steps resulted in a final list of 1,217 high-confidence peaks located near 1,106 genes (Supplemental Table S5D).

To obtain a broad view of the function of the ZmAN3 target genes, a GO enrichment analysis was performed on the 1,106 genes bound by ZmAN3 (Supplemental Table S5E), clearly supporting its role in leaf growth and development. The most significantly enriched biological process, however, was regulation of transcription (hypergeometric test, $P = 9.59E-16$), an observation that was strengthened by the significant overlap with two maize TF databases (Yilmaz et al., 2009; Jin et al., 2017) showing that almost one-fifth of the peaks (237 out of 1,217) mapped to a gene encoding a TF (hypergeometric test, $P = 1.37E-47$; Supplemental Table S5D). This is in agreement with observations made in the two AN3 benchmark studies. Several enriched GO terms further validate the observation made in the maize tassel study that ZmAN3 also has a preference to regulate hormone-related genes (Zhang et al., 2018).

To investigate the functional conservation of ZmAN3 across different maize tissues, the maize leaf ChIP-seq data were compared with the ZmAN3 target genes that were identified recently in developing tassels by ChIP-seq and transcriptome analyses (Zhang et al., 2018). Whereas a small but significant overlap was detected between the leaf and tassel ChIP-seq data sets (hypergeometric test, $P = 4.66E-02$), 14.5% of the leaf ChIP targets were differentially expressed in the tassel of the *ZmAN3* mutant line, representing a highly significant overlap (hypergeometric test, $P = 1.23E-50$; Fig. 6A; Supplemental Table S5D). This not only pinpoints the high quality of the leaf ChIP data but, in addition, indicates that ZmAN3 regulates similar genes in the leaf growth zone and in developing tassels. Many interesting genes were present in this overlap, such as GRMZM2G399072, an ortholog of *AINTEGUMENTA*, encoding a key regulator of final leaf and flower size in Arabidopsis (Mizukami and Fischer, 2000; Krizek, 2009). This gene was one of the most strongly enriched genes (rank 8) when the ChIP data set was sorted according to the average fold enrichment over the four experiments (Supplemental Table S5D). Another common gene was GRMZM2G445169, encoding an expansin (EXPA4) involved in cell expansion. This indicates that ZmAN3 might directly regulate cell expansion, as further demonstrated by the presence of five additional expansin genes specifically found in the leaf ChIP data, of which two were among the most highly enriched genes (EXPA8, rank 4, and EXPB4, rank 17; Supplemental Table S5D). The leaf ChIP data also support the tassel transcriptome data set in that ZmAN3 regulates genes involved in cell proliferation, as witnessed by the strong binding in the promoter region of the D-type cyclin cell cycle regulator *ZmCycD7;1* (rank 92; Fig. 6B). Finally, the presence of two GRFs (*ZmGRF3* and *ZmGRF17*) in the overlap reinforces the existence of transcriptional feedback mechanisms, which were reported previously in both Arabidopsis and maize (Vercruyssen et al., 2014; Zhang et al., 2018). Intriguingly, the expression of *ZmGRF17* was down-regulated in the *ZmAN3* tassel mutant, whereas the expression of *ZmGRF3* was up-regulated. In addition, we also identified binding to two other GRFs (*ZmGRF1* and *ZmGRF9*), which might reflect specific targets of ZmAN3 in the leaf. The underlying feedback mechanisms might be even more complex, as demonstrated by the presence of several TEOSINTE BRANCHED1/CYCLOIDEA/PCF (TCP) TF members in the leaf ChIP data (Fig. 6B; Supplemental Table S5D), which are known to activate the expression of the microRNA *miR396b* that targets GRF transcripts (Schommer et al., 2014; Omidbakhshfard et al., 2015).

To shed light on the overall conservation of the AN3 DNA-binding landscape across dicots and monocots, Arabidopsis orthologs of the maize ZmAN3 targets were stringently identified and compared with the Arabidopsis TChAP targets (Vercruyssen et al., 2014). This analysis revealed that more than one-third (36%) of the maize *AN3* targets for which an Arabidopsis ortholog could be determined were present in the Arabidopsis TChAP-seq data (Fig. 6A; Supplemental Table S5F). This reflects a highly significant overlap (hypergeometric test, $P = 1.53E-73$) and illustrates the functional conservation of AN3 target genes between monocots and dicots. A GO enrichment analysis (Supplemental Table S5G) of these conserved target genes confirmed the role of AN3 as an upstream regulator of TFs (GO:0003700, $P = 9.91E-08$) and as a regulator of leaf growth and development (e.g. GO:0040007, growth, $P = 7.18E-06$; GO:0048367, shoot system development, $P = 1.00E-03$; Supplemental Table S5H). However, one of the most strongly enriched GO terms among the conserved targets was response to hormone (GO:0009725, $P = 2.55E-19$), supporting observations reported earlier in the ZmAN3 tassel study (Zhang et al., 2018). This shows the functional conservation of ZmAN3 across different plant species as a master regulator of an extended downstream transcriptional network as well as a regulator of hormonal responses and of genes involved in leaf growth and development.

In summary, the conserved features of the AN3 DNA-binding landscape between different maize tissues and across monocots and dicots reflect the high quality of the maize leaf ChIP data, demonstrating that the GS^{yellow} tag can be used for ChIP analyses on specific tissues of maize.

DISCUSSION

In this study, a multifunctional GS^{yellow} tag was developed to identify protein-protein and protein-DNA interactions while simultaneously allowing the gathering of information on the subcellular localization pattern of the bait of interest from a single transformed line. This Swiss-knife approach of performing multiple types of experiments on a single transgenic line is advantageous because it avoids extra cloning and transformation work, which is particularly interesting for plant species for which the throughput of transformation is limited. Moreover, because variation in the positional effects of transgene insertion is eliminated when

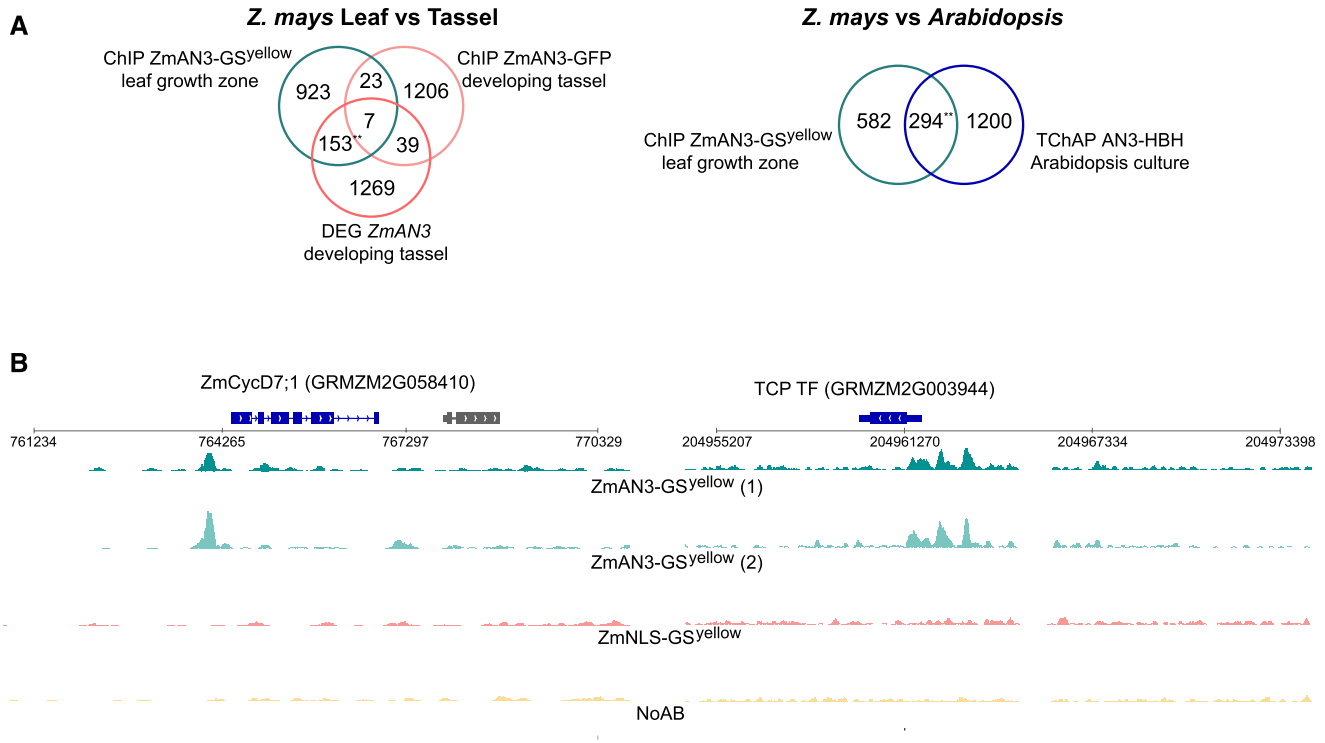

Figure 6. Analysis of ZmAN3-GS^{yellow} leaf ChIP targets. A, The first Venn diagram represents the significant overlap of the ZmAN3-GS^{yellow} maize leaf ChIP data with genes differentially expressed (DEG) in the tassel of the *ZmAN3* mutant (hypergeometric test, P = 1.23E-50) or with genes identified by ChIP in the tassel using ZmAN3-GFP. In the second Venn diagram, the significant overlap (hypergeometric test, P = 1.53E-73) is shown between the leaf ZmAN3-GS^{yellow} ChIP targets and the Arabidopsis cell culture TChAP targets, taking only genes into account for which an ortholog could be determined. ** = highly significant overlap. B, Sashimi plot obtained from the Integrative Genomics Viewer, demonstrating the binding of ZmAN3 to the promoter regions of ZmCycD7;1 (GRMZM2G058410) and TCP TF (GRMZM2G003944). The sequence reads of both ZmAN3 replicates and of the two control samples (ZmNLS and NoAB) are shown. The ZmCycD7;1 and TCP gene regions are represented by blue bars.

working on a single transgenic line, it enables a more accurate comparison of data obtained from different types of experiments.

For protein complex analysis, the main advantage of the GS^{yellow} tag compared with a single GFP tag resides in its flexibility to explore protein-protein interactions through TAP, delivering protein complexes of high purity, which is advantageous for the detection of strong substoichiometric interactions and for further downstream analysis (Van Leene et al., 2015). Moreover, because of the presence of the cYFP moiety, the GS^{yellow} tag also can be used for single-step GFP-based affinity purification methods (Smaczniak et al., 2012; Wendrich et al., 2017), increasing the chance of detecting weak interactions in case these would be lost during TAP. As such, the GS^{yellow} tag offers a versatile tool for protein complex analysis by applying either a single affinity purification or a TAP protocol, while maintaining the possibility to perform subcellular localization and anti-GFP-based ChIP-seq analyses.

To analyze the efficiency of the GS^{yellow} tag, several benchmark proteins were selected in Arabidopsis and maize. Through complementation analysis, we show that the GS^{yellow} tag does not cause sterical hindrance or impede the functionality of the tested bait proteins. Moreover, the confirmation of known interaction partners or known target genes indicates that the GS^{yellow} tag performs comparable to the available alternatives. For TAP using AN3 and PPD2 as bait proteins in Arabidopsis cell cultures, the GS^{yellow} tag even slightly outperformed the GS^{rhino} TAP results.

The performance of the GS^{yellow} tag for ChIP in plants was demonstrated by the extensive overlap of PPD2- or ZmAN3-GS^{yellow} target genes with previously reported target genes (Vercruyssen et al., 2014; Zhang et al., 2018). Interestingly, the maize ZmAN3 ChIP-seq results revealed that not only the association of AN3 with the SWI/SNF complex and GRFs is conserved across dicots and monocots (Nelissen et al., 2015) but also its target genes. Moreover, it appeared that these conserved target genes are highly enriched for TFs, shedding light on how AN3 acts as a conserved master regulator of downstream transcriptional networks. Although the binding of ZmAN3 to genes encoding GRFs and TCPs shows the existence of complex regulatory feedback loops, follow-up research is required to

clarify the exact nature of these regulatory mechanisms. In addition to the identification of conserved targets, many novel maize-specific targets were found. These might have been missed in the Arabidopsis TChAP-seq data because of the cell culture context, whereas in this study, binding was assessed in the endogenous context of ZmAN3 in the leaf growth zone. Conversely, comparison of the ZmAN3 leaf ChIP data with genes that are differentially expressed in the developing tassel of a *ZmAN3* mutant (Zhang et al., 2018) showed a high degree of conservation among ZmAN3 target genes across different tissues. In future research, it will be interesting to exploit the ZmAN3-GS^{yellow} fusion for dynamic mapping of the gene regulatory networks acting in the different growth zones of the developing maize leaf. This will provide more insight into how ZmAN3 targets different genes through its dynamic interaction with GRFs or other TFs and, ultimately, should contribute to our understanding of how AN3 regulates leaf growth and development in plants.

In conclusion, we demonstrated that the GS^{yellow} molecular toolbox provides added value for functional studies of proteins in plant model species and crops and should further boost the output of plant research.

MATERIALS AND METHODS

Construction of Entry Clones

Primer sequences used for cloning are listed in Supplemental Table S6. The production of the following entry clones through the Gateway recombination method (Invitrogen) is described elsewhere: pEN-L1L2_AN3 (Vercruyssen et al., 2014), pEN-L4R1_proLat52 and pEN-L1L2_TPLATE (Van Damme et al., 2006), pEN-L1L2_PPD2 (Gonzalez et al., 2015), pEN-L1L2_NLS and pEN-L4R1_proUBIL (Karimi et al., 2007), and pEN-L1L2_ZmAN3 (Nelissen et al., 2015). For ZmNLS (Varagona et al., 1992), pEN-L1L2_ZmNLS was constructed through overlap PCR with attB1_ZmNLS_Fwd and attB2_ZmNLS_Rev primers and cloned into pDONR221 via a BP reaction.

The GS^{yellow} tags were constructed as follows. For the C-terminal GS^{yellow} tag, we first isolated cYFP DNA from DR5:PIN-cYFP maize plants (Mohanty et al., 2009) and amplified it using SBP+cYFP_Fwd and attB3_GFP/cYFP_Rev primers. In parallel, we amplified the SBP-TEV2-Rh3C2 fragment from pEN-L1L2-GS^{green} (Blomme et al., 2017) using attB2R_Gly4Ser_linker_Fwd and SBP+cYFP_Rev primers. Both PCR products were then combined using extension overlap PCR and cloned into pDONRP2RP3 to produce pEN-R2L3-GS^{yellow}. The N-terminal GS^{yellow} tag was synthesized in pUC57 as attB1-Ωleader-cYFP-Rh3C$_2$-TEV$_2$-SBP-G4S-attB2 and cloned directly into pDONR221 using a BP reaction to produce pEN-L1L2_NGS^{yellow}. The pUC57 vector also was used as a template for an adaptor PCR with attB4/attB1R Gateway sites. The resulting PCR product was cloned into pDONRP4P1R to produce pEN-L4L1R-NGS^{yellow}.

Construction of the organelle-targeting peptide variants was carried out as follows. NLS (for nuclear targeting), mitochondrial, chloroplast, and 2S2 (for ER targeting) N-terminal GS^{rhino} and GS^{yellow} targeting peptide TAP tag sequences were synthesized with minor codon adaptations and flanked by attB1/attB2 Gateway recombination sites. The sequences for the organelle-targeting peptides were respectively obtained from pEN-L1L2-NF (Karimi et al., 2007), Arabidopsis 2S2 albumin (Krebbers et al., 1988), the E1 α-subunit of plastid pyruvate dehydrogenase (Lee et al., 2009), and the cytochrome *c* oxidase subunit 4 of *Saccharomyces cerevisiae* (Nelson et al., 2007). Synthesized fragments were used in standard Gateway BP reactions with pDONR221 to obtain attL1/attL2 entry vectors. The resulting vectors were used as templates for adaptor PCR and transfer of the tags to pDONRP4P1R. All generated Gateway entry vectors are listed in Supplemental Table S7.

Construction of Expression Vectors

35S:ORF-tag or 35S:tag-ORF constructs were generated as described previously (Van Leene et al., 2011). The organelle-targeting NGS^{rhino} expression vectors were produced through multisite Gateway LR reaction with pEN-L4R1-2 (p35S) and pEN-R2L3-F (GFP) entry vectors into the pK7m34GW destination vector (Karimi et al., 2007). pLat52:TPLATE-GS^{yellow} was produced through multisite Gateway LR reaction with the corresponding entry vectors and the pB7m34GW destination vector. pUBIL:ZmAN3-GS^{yellow} was constructed using the pBb7m34GW destination vector (Karimi et al., 2013). All obtained Gateway expression vectors are listed in Supplemental Table S7.

Plant Materials, Growth Conditions, and Growth Measurements

PSB-D Arabidopsis (*Arabidopsis thaliana* ecotype Landsberg *erecta*) cell suspension cultures were transformed with 35S:ORF-tag constructs as described previously (Van Leene et al., 2011). Transformation of Arabidopsis (ecotype Columbia-0) plants was carried out through standard floral dip. 35S:AN3-GS^{yellow} was transformed into the wild-type background, and transgenic offspring were selected on one-half-strength Murashige and Skoog medium supplemented with kanamycin. Arabidopsis seedlings that expressed 35S:AN3-GS^{yellow} were grown in vitro for 6 d on one-half-strength Murashige and Skoog medium supplemented with 1% (w/v) Suc. pLat52:TPLATE-GS^{yellow} was transformed into the SALK_0030086 heterozygous mutant background, and transformants were selected on one-half-strength Murashige and Skoog medium supplemented with Basta. For TAP, Arabidopsis seedlings were grown as described previously (Van Leene et al., 2015). Analysis of the overexpressor phenotype of the *AN3* lines was carried out as described previously (Vercruyssen et al., 2014). Briefly, plants were grown for 21 d in vitro on one-half-strength Murashige and Skoog medium supplemented with 1% (w/v) Suc at 21°C under a 16-h-day/8-h-night regime. Leaf areas were measured with ImageJ (https://imagej.net/Welcome) after dissection of individual leaves.

For maize (*Zea mays*) experiments, a B104 inbred line was transformed with pUBIL:ZmAN3-GS^{yellow} via *Agrobacterium tumefaciens*-mediated transformation of immature embryos (Coussens et al., 2012). Fifteen transgenic lines were backcrossed to B104, from which one line, named ZmAN3-GS^{yellow}, containing a single T-DNA locus and showing protein expression on western blot, was retained for all further analyses. Segregating offspring were identified using either the PAT assay (AgraStrip LL), which tests for *bar* marker gene activity, or through scoring of the fluorescent GS^{yellow} signal in the root tip (Supplemental Fig. S4). Plants were grown and harvested as described previously (Nelissen et al., 2015). Detection of GS^{yellow}-tagged proteins was performed with ab290 anti-GFP (Abcam). Growth analyses were performed as described (Nelissen et al., 2013).

Analysis of *TPLATE* Complementation through Genotyping and Scanning Electron Microscopy

Genotyping PCR to analyze the *TPLATE* T-DNA insertion locus (SALK_0030086) was carried out as described previously (Van Damme et al., 2006). Segregation analysis of heterozygous *TPLATE* mutants and heterozygous *TPLATE* mutants homozygous for *pLat52:TPLATE-GS^{yellow}* was checked via PCR. To study pollen viability by scanning electron microscopy, air-dried pollen from wild-type (Col-0), heterozygous *TPLATE* mutants, and heterozygous *TPLATE* mutants homozygous for *pLat52:TPLATE-GS^{yellow}* were taped on stubs and examined with a Hitachi table-top microscope (TM-1000; Hitachi High-Technologies Europe) under a 15-kV acceleration voltage. Quantification of pollen morphology (ratios of shriveled versus normal pollen) was performed via visual scoring of the phenotype based on the scanning electron microscopy images acquired.

TAP

Arabidopsis cell culture and seedling TAP experiments were carried out as described previously (Van Leene et al., 2015), applying minor adaptations for the GS^{yellow} TAPs. Briefly, protein extracts were derived from 2.5 g of harvested cells or 50 g of 6-d-old seedlings grown in liquid one-half-strength Murashige and Skoog medium. For TAP, 25 mg (cell culture) or maximum (seedlings, using equal input for duplicates) total protein was used as input, and complexes were purified using 25 µL of IgG-Sepharose (GS^{rhino}) or anti-GFP agarose beads

(GS^{yellow}; GFP-Trap-A; Chromotek). After binding, complexes were eluted using 10 units of rhinovirus 3C protease and further isolated on 25-µL streptavidin beads as described (Van Leene et al., 2015). For cell culture TAPs, purified proteins were eluted with 30 µL of 1× NuPAGE sample buffer (Invitrogen), supplemented with 20 mM desthiobiotin. For seedling TAPs, proteins were eluted in 1 mL of streptavidin elution buffer and concentrated by TCA precipitation. The protein pellet was resolved in 30 µL of 1× NuPAGE sample buffer. Proteins were separated on NuPAGE Bis-Tris gels (Invitrogen). TAPs on maize were executed as described previously (Nelissen et al., 2015); however, the amount and type of the beads used follow the GS^{yellow} Arabidopsis cell culture TAP protocol, starting from 5 g of maize leaf tissue (leaf 4, growth zone from cm 1 to 4).

Liquid Chromatography-Tandem MS Analysis

After separation, proteins were Coomassie blue stained and in-gel digested with trypsin as described previously (Van Leene et al., 2015). The digested peptide mixtures were injected into a liquid chromatography-tandem MS system using an Ultimate 3000 RSLCnano LC (Thermo Fisher Scientific) in-line connected to either an LTQ Orbitrap Velos (Thermo Fisher Scientific; for the Arabidopsis samples) or a Q Exactive mass spectrometer (Thermo Fisher Scientific; for the maize samples), as described previously (Nelissen et al., 2015). Briefly, peptides were separated through a 30-min linear gradient from 98% solvent A9 (0.1%[v/v] formic acid in water) to 40% solvent B9 (0.1% [v/v] formic acid in water:acetonitrile, 20:80 [v/v]), and for each MS1 scan, the 10 most abundant ions were chosen for fragmentation.

MS Data Analysis

For the Arabidopsis samples, a Mascot generic file was created using Mascot Distiller (version 2.4.3.1 for the AN3 and TPLATE cell culture samples, and version 2.5 for the PPD2 cell culture samples and the seedling samples). Spectra with a maximum intermediate retention time of 30 s and a maximum intermediate scan count of five were grouped, if possible, using a 0.005-D precursor tolerance. Deisotoping was deactivated, and a relative signal-to-noise limit was set at 2. A peak list was generated only when the MS/MS spectrum contained more than 10 peaks. The peak list was then searched against the TAIRplus database (accessible at http://www.psb.ugent.be/tapdata), which is an extended version of the TAIR10 database that also contains sequences of all types of non-TAIR contaminants in TAP or other proteomics experiments. Included in these contaminants are the cRAP protein sequences that originate from proteins that were copurified by accident or from contaminating proteins that are unavoidably present in protein samples (The Global Proteome Machine; http://www.thegpm.org/crap/). The searches were carried out using the Mascot search engine (version 2.4.1 for the AN3 and TPLATE cell culture samples, and version 2.5.1 for the PPD2 cell culture samples and the seedling samples) with the following parameters: variable modifications, oxidation (Met) and methyl (Asp); fixed modification, carbamidomethyl (Cys); enzyme, trypsin/Pro; maximum missed cleavages, 1; charge, 2^+ and 3^+; peptide tolerance, 10 ppm; # ^{13}C, 1; MS/MS tolerance, 0.5 D; instrument, ESI-TRAP. The Mascot data were then selected using a significance threshold of $P < 0.01$, with the maximum number of hits set to AUTO. Results were filtered in Excel for rank 1 peptides. Only identifications from Arabidopsis (TAIR10; this is the implemented database for all Arabidopsis searches) with at least two matched high-confidence rank 1 peptides, of which at least one is unique to the protein, were retained.

For the maize samples, the raw files were processed in two sets (leaf division zone versus leaf expansion zone) using MaxQuant software (version 1.5.3.28; Cox and Mann, 2008). The data were searched against the Z.mays.AGPv3.27.pep.all database (downloaded from ftp.ensemblgenomes.org) using the built-in Andromeda search engine. A complete list of the MaxQuant search parameters is provided in Supplemental Table S8. A target-decoy approach with a false discovery rate of 1% was used to filter protein identifications and Peptide-Spectra Matches. Supplemental Table S4A contains the proteingroups output file from MaxQuant.

Correcting for False Positives and Nonspecific Protein Interactors

Besides specific, bona fide interactors, TAP experiments also copurify nonspecific interactors that interact with many unrelated bait proteins as well as false positive interactors that bind the resin instead of the bait protein. Discriminating between such specific and nonspecific or false positive interactors is generally carried out by performing a large series of TAP experiments with a wide variety of baits to determine bait-independent recurring copurifying proteins (Keilhauer et al., 2015; Van Leene et al., 2015). For the Arabidopsis TAPs, we used an updated version of the previously published Arabidopsis background list (Van Leene et al., 2015). This list was constructed by performing 802 TAP experiments on 163 different baits that were tagged with the GS tag and expressed in Arabidopsis cell cultures or seedlings. These baits were further subdivided into 87 groups, based on their co-occurrence in the same protein complex (if this information was available) or on their involvement in the same biological process as assessed by their gene ontology. Proteins present in three or more bait groups were considered nonspecific and were used to create the updated nonspecific list containing 936 entries (Supplemental Table S1B). For each TAP experiment, possible interactors of the bait of interest were identified by filtering out proteins present in this background list. To avoid the loss of bona fide interactors in TAP experiments, semiquantitative analysis based on normalized spectral abundance factor (NSAF) was used. For each identification, an NSAF value was calculated by normalizing the total number of spectra that matched the protein by its length and by the total number of matched spectra in the sample. Identifications with an NSAF ratio > 10 versus the average NSAF of the same protein in the data set of 802 TAP experiments used for construction of the background list were retained as bona fide interactors, despite their presence in the background list.

For the maize TAPs, first, identifications in columns only identified by site, reverse, and contaminant, in the protein groups list (Supplemental Table S4A), were filtered away. Background filtering was done in two steps as described before (Nelissen et al., 2015). Therefore, the previously published maize background list was updated with two mock GS^{yellow} purifications on wild-type B104 protein extracts obtained from the ear. From these mock purifications, all proteins that were identified with at least one high-confidence peptide with Q Exactive were used to build the extended maize background list (Supplemental Table S4B). This list was then used to filter nonspecific proteins from the TAP experiments on ZmAN3-GS^{yellow}. In addition, the Arabidopsis orthologs of all proteins that were identified in the maize TAP experiments were determined via PLAZA 3.0 dicots (Proost et al., 2015). If the Arabidopsis ortholog was known to be in the background of Arabidopsis, the maize protein also was considered as a nonspecific interactor and filtered out of the maize TAP data. All proteins that were filtered out in this manner are listed in Supplemental Table S4C. Finally, only proteins that were identified with at least two peptides, of which at least one was unique, were retained (Table III; Supplemental Table S4D).

MaxLFQ of Leaf ZmAN3 TAP Samples

For all ZmAN3-GS^{yellow} TAP samples, proteins were quantified in a relative manner using the MaxLFQ algorithm (Cox et al., 2014) that is integrated in the MaxQuant software. Here, only proteins identified with at least one unique peptide were used, and MaxLFQ values were determined only with unique peptides. Minimum LFQ ratio counts were set to 1, and the data were analyzed with the Perseus software (version 1.5.1.6). The proteingroups file (Supplemental Table S4A) obtained from MaxQuant was loaded into Perseus, and all LFQ intensity values were $\log_2$ transformed. Reverse database hits, proteins identified only by site and contaminants, were filtered out. The ZmAN3 TAP samples were grouped into division zone (five TAPs) and expansion zone (five TAPs). To improve confidence levels, proteins that did not show four valid values in at least one of the groups were removed. For missing values, a value was imputed based on a normal distribution around the detection limit of the mass spectrometer. We then performed Student's *t* test to assess statistical outliers between the expansion and division zone groups. To correct for the multiple hypothesis problem, a permutation-based false discovery rate correction was used. The division zone-specific, significantly enriched proteins identified with Student's *t* test can be found in Supplemental Table S4E.

Microscopy

For pLat52:TPLATE-GS^{yellow}, spinning disc confocal microscopy (Perkin Elmer Ultraview system on an inverted Nikon Ti microscope) of endocytic foci and kymograph processing were carried out on hypocotyl cells as described previously (Gadeyne et al., 2014). Time series were acquired for 3 min, with one time point per second. Excitation was done at 514 nm, exposure was set

to 500 ms, and emission was detected between 525 and 575 nm [Ultraview Emission wheel set to 550(W49)]. ImageJ (Fiji) was used for image processing. Background subtraction was achieved with a five-pixel rolling ball radius, and walking averages of two subsequent frames were applied. Kymographs with a line width of three pixels were made using the Kymograph2 plugin, and the lifetime of individual endocytic foci was measured manually from the generated kymographs (n = 964).

Proteins tagged with different organelle-targeting peptide variants were transiently transformed in tobacco (*Nicotiana tabacum*) leaf cells and expressed from a 35S promoter. Localization was analyzed using an LSM 710 inverted confocal microscope (Zeiss) equipped with one of the following objectives: C-Apochromat 40×/1.2 W Corr M27 objective for Mito_GS^{rhino}-GFP, EC Plan-Neofluar 10×/0.3 objective for NLS_GS^{rhino}-GFP, C-Apochromat 63×/1.2 W Corr M27 objective for ER_GS^{rhino}-GFP, and EC Plan-Neofluar 20×/0.5 objective for Chl_GS^{rhino}-GFP. Excitation was carried out at 488 nm for GFP and 543 nm for RFP signals. Emission was detected between 505 and 530 nm for GFP and between 560 and 615 nm for RFP. For the detection of Mito_GS^{rhino}-GFP, tobacco leaf samples were analyzed 30 min after infiltration with infiltration buffer containing MitoTracker Red CM-H2XRos (Molecular Probes, Life Technologies) 4 d after agroinfiltration of the constructs.

Transgenic pUBIL:ZmAN3-GS^{yellow} maize offspring were identified through the YFP signal in the root tip of germinating seedlings 1 week after sowing in a Jiffy-7 pellet (Supplemental Fig. S4). Screening for YFP fluorescence was carried out with a 1× lens on an MZ16 fluorescence stereomicroscope (Leica Microsystems) equipped with a blue light source and a Leica GFP Plus filter set. Images were obtained through an AxioCam HRc from Zeiss.

Confocal microscopy of 35:AN3-GS^{yellow} in Arabidopsis seedlings and of pUBIL:ZmAN3-GS^{yellow} in maize was carried out with a FluoView1000 inverted confocal microscope (Olympus) equipped with a water-corrected 60× objective (numerical aperture 1.2). cYFP was excited at 515 nm, and its emission was detected between 530 and 560 nm.

ChIP-Seq

ChIP-seq on PPD2-GS^{yellow} and ZmAN3-GS^{yellow} was performed using 5 µL of ab290 anti-GFP antibody (Abcam), with minor adaptations of a published protocol (Morohashi et al., 2012). For each maize sample, 1.2 g of leaf tissue (cm 1–4 of leaf 4) was fixed in buffer A for 15 min under vacuum conditions. For quenching, Gly was added to a final concentration of 0.1 M and incubated for 10 min. Fixed leaf tissue was washed with distilled water and frozen in liquid N_2. Cross-linking of Arabidopsis cell culture material was carried out as described previously (Verkest et al., 2014), and 1 g of fixed material was used per ChIP. All subsequent steps were carried out as described by Morohashi et al. (2012). ChIP-seq library preparation and Illumina sequencing (HiSeq2500; http://www.illumina.com/applications/sequencing.html) were performed by GATC Biotech. In total, 20 million reads were carried out per sample, with 50-bp-long single-end and 125-bp-long paired-end reads for Arabidopsis cell culture or maize samples, respectively, generating the ChIP-seq data as represented in Supplemental Table S9. The Arabidopsis ChIP-seq data were processed as described previously (Van Leene et al., 2016). Briefly, for peak calling, MACS version 2.1.1 was used with an effective genome size of 100 Mb, MFold parameters [10, 30], and q value of 0.05 (Zhang et al., 2008). PPD2-GS^{yellow} was normalized against an NLS-GS^{yellow} control and the new or published (Gonzalez et al., 2015) PPD-HBH samples against a mock wild-type control. Peaks in common between two repeats were identified using intersectBed from the BEDTools utility with at least 25% overlap (-f 0.25; Quinlan and Hall, 2010). To determine the overlap of the intersects, peaks that shared their summits within a distance of 250 bp (approximately half of the medium peak length) were retained, based on the coordinates of the first sample. For de novo motif finding among PPD2 peaks, peak-motifs from RSATools was used with oligos, positions, and local_words as the discovery algorithms (http://rsat01.biologie.ens.fr/rsat/tutorials/tut_peak-motifs.html). For the maize ChIPs, data were analyzed in Galaxy according to the pipeline shown in Supplemental Figure S5. The quality of raw reads was checked using FASTQC (http://www.bioinformatics.babraham.ac.uk/projects/fastqc) version 0.51. The reads were mapped using BWA version 1.2.3 using setting pre_set (Li and Durbin, 2009). Only reads that were uniquely mapped were used for further analyses. Peak calling was done using MACS version 2.1.1 with an effective genome size of 1,920 Mb, MFold parameters [10, 30], and q value of 0.05 (Zhang et al., 2008). Both ZmAN3 samples were normalized against the NLS-GS^{yellow} and NoAB controls separately. Peaks were annotated to the closest genes in the ZmB73_5b.60 version of the genome. Peaks in common between two repeats were identified with at least 50% overlap (-f 0.5). GO enrichments were analyzed through the PLAZA 3.0 Monocots platform (Proost et al., 2015). To determine the overlap of the intersects against the two negative controls, peaks that shared their summits within a distance of half the medium peak length were retained, based on the coordinates of the first sample. To analyze the overlap between the maize ZmAN3 ChIP data and the Arabidopsis AN3-related TChAP and transcriptome data, Arabidopsis orthologs of the ZmAN3 targets were identified through the PLAZA integrative method (PLAZA 3.0, Monocots) using all possible orthologous relations (M = N = 1; M = 1, N > 1; M > 1, N = 1; M > 1, N > 1). For stringent identification of orthologs (Supplemental Table S5E), two rules were applied: (1) used evidence = TROG, required number of evidences = 1 or more; (2) used evidence = TROG, BHIF, ORTHO, required number of evidences = 2 or more. To analyze the statistical significance of overlaps, a hypergeometric function was used.

Accession Numbers

Sequence data from this article can be found in the GenBank/EMBL data libraries under accession numbers AT5G28640 (AN3), AT4G14720 (PPD2), AT3G01780 (TPLATE), and NM_001112560 (ZmAN3). The PPD2 and ZmAN3 ChIP-seq data have been deposited in the ArrayExpress database (http://www.ebi.ac.uk/arrayexpress) under accession numbers E-MTAB-6513 and E-MTAB-6527, respectively.

Supplemental Data

The following supplemental materials are available.

Supplemental Figure S1. Annotated DNA and amino acid sequence overview of the N-terminal GS^{yellow} tag.

Supplemental Figure S2. Organelle-targeting peptide GS^{rhino} TAP tag variants, fused to GFP.

Supplemental Figure S3. Phenotypical analysis comparing the final leaf length (leaf 4) of the transgenic pUBIL:ZmAN3-GS^{yellow} maize plants with that of their nontransgenic counterparts.

Supplemental Figure S4. Screening of transgenic maize root tips expressing pUBIL:ZmAN3-GS^{yellow} through fluorescence microscopy of the emerging root tips of maize, 3 d after sowing.

Supplemental Figure S5. Schematic representation of the ZmAN3-GS^{yellow} ChIP-seq data-processing pipeline in Galaxy.

Supplemental Table S1. Results of Arabidopsis TAP analyses.

Supplemental Table S2. Results of PPD2 ChIP-seq analysis.

Supplemental Table S3. PPD2 ChIP data GO analysis.

Supplemental Table S4. TAP results for ZmAN3-GS^{yellow}.

Supplemental Table S5. ZmAN3-GS^{yellow} ChIP-seq analysis results in maize.

Supplemental Table S6. List of primers used for cloning.

Supplemental Table S7. Summary of used Gateway entry and expression vectors.

Supplemental Table S8. MaxQuant search parameters.

Supplemental Table S9. Summary of read, peak, and gene number of PPD2 and ZmAN3 ChIP-seq experiments.

ACKNOWLEDGMENTS

We thank Annick Bleys for help in preparing the article, Frederik Coppens for help with the data submission, and Astrid Gadeyne for assistance with confocal microscopy.

Received February 9, 2018; accepted April 1, 2018; published April 20, 2018.

LITERATURE CITED

Blomme J, Van Aken O, Van Leene J, Jégu T, De Rycke R, De Bruyne M, Vercruysse J, Nolf J, Van Daele T, De Milde L, (2017) The mitochondrial DNA-associated protein SWIB5 influences mtDNA architecture and homologous recombination. Plant Cell **29**: 1137–1156

Bunnik EM, Le Roch KG (2013) An introduction to functional genomics and systems biology. Adv Wound Care (New Rochelle) **2**: 490–498

Bürckstümmer T, Bennett KL, Preradovic A, Schütze G, Hantschel O, Superti-Furga G, Bauch A (2006) An efficient tandem affinity purification procedure for interaction proteomics in mammalian cells. Nat Methods **3**: 1013–1019

Cheeseman IM, Desai A (2005) A combined approach for the localization and tandem affinity purification of protein complexes from metazoans. Sci STKE **2005**: pl1

Coussens G, Aesaert S, Verelst W, Demeulenaere M, De Buck S, Njuguna E, Inzé D, Van Lijsebettens M (2012) *Brachypodium distachyon* promoters as efficient building blocks for transgenic research in maize. J Exp Bot **63**: 4263–4273

Cox J, Mann M (2008) MaxQuant enables high peptide identification rates, individualized p.p.b.-range mass accuracies and proteome-wide protein quantification. Nat Biotechnol **26**: 1367–1372

Cox J, Hein MY, Luber CA, Paron I, Nagaraj N, Mann M (2014) Accurate proteome-wide label-free quantification by delayed normalization and maximal peptide ratio extraction, termed MaxLFQ. Mol Cell Proteomics **13**: 2513–2526

Cuéllar Pérez A, Nagels Durand A, Vanden Bossche R, De Clercq R, Persiau G, Van Wees SCM, Pieterse CMJ, Gevaert K, De Jaeger G, Goossens A, (2014) The non-JAZ TIFY protein TIFY8 from *Arabidopsis thaliana* is a transcriptional repressor. PLoS ONE **9**: e84891

Debernardi JM, Mecchia MA, Vercruyssen L, Smaczniak C, Kaufmann K, Inzé D, Rodriguez RE, Palatnik JF (2014) Post-transcriptional control of *GRF* transcription factors by microRNA miR396 and GIF co-activator affects leaf size and longevity. Plant J **79**: 413–426

Dedecker M, Van Leene J, De Jaeger G (2015) Unravelling plant molecular machineries through affinity purification coupled to mass spectrometry. Curr Opin Plant Biol **24**: 1–9

De Souza CP, Hashmi SB, Osmani AH, Osmani SA (2014) Application of a new dual localization-affinity purification tag reveals novel aspects of protein kinase biology in *Aspergillus nidulans*. PLoS ONE **9**: e90911

Gadeyne A, Sánchez-Rodríguez C, Vanneste S, Di Rubbo S, Zauber H, Vanneste K, Van Leene J, De Winne N, Eeckhout D, Persiau G, (2014) The TPLATE adaptor complex drives clathrin-mediated endocytosis in plants. Cell **156**: 691–704

Gonzalez N, Pauwels L, Baekelandt A, De Milde L, Van Leene J, Besbrugge N, Heyndrickx KS, Cuéllar Pérez A, Durand AN, De Clercq R, (2015) A repressor protein complex regulates leaf growth in *Arabidopsis*. Plant Cell **27**: 2273–2287

Goossens J, De Geyter N, Walton A, Eeckhout D, Mertens J, Pollier J, Fiallos-Jurado J, De Keyser A, De Clercq R, Van Leene J, (2016) Isolation of protein complexes from the model legume *Medicago truncatula* by tandem affinity purification in hairy root cultures. Plant J **88**: 476–489

Griesbeck O, Baird GS, Campbell RE, Zacharias DA, Tsien RY (2001) Reducing the environmental sensitivity of yellow fluorescent protein: mechanism and applications. J Biol Chem **276**: 29188–29194

Horiguchi G, Kim GT, Tsukaya H (2005) The transcription factor AtGRF5 and the transcription coactivator AN3 regulate cell proliferation in leaf primordia of *Arabidopsis thaliana*. Plant J **43**: 68–78

Horiguchi G, Nakayama H, Ishikawa N, Kubo M, Demura T, Fukuda H, Tsukaya H (2011) *ANGUSTIFOLIA3* plays roles in adaxial/abaxial patterning and growth in leaf morphogenesis. Plant Cell Physiol **52**: 112–124

Jin J, Tian F, Yang DC, Meng YQ, Kong L, Luo J, Gao G (2017) PlantTFDB 4.0: toward a central hub for transcription factors and regulatory interactions in plants. Nucleic Acids Res **45**: D1040–D1045

Karimi M, Bleys A, Vanderhaeghen R, Hilson P (2007) Building blocks for plant gene assembly. Plant Physiol **145**: 1183–1191

Karimi M, Inzé D, Van Lijsebettens M, Hilson P (2013) Gateway vectors for transformation of cereals. Trends Plant Sci **18**: 1–4

Kawade K, Horiguchi G, Usami T, Hirai MY, Tsukaya H (2013) ANGUSTIFOLIA3 signaling coordinates proliferation between clonally distinct cells in leaves. Curr Biol **23**: 788–792

Keilhauer EC, Hein MY, Mann M (2015) Accurate protein complex retrieval by affinity enrichment mass spectrometry (AE-MS) rather than affinity purification mass spectrometry (AP-MS). Mol Cell Proteomics **14**: 120–135

Kim JH, Kende H (2004) A transcriptional coactivator, AtGIF1, is involved in regulating leaf growth and morphology in *Arabidopsis*. Proc Natl Acad Sci USA **101**: 13374–13379

Kobayashi T, Morone N, Kashiyama T, Oyamada H, Kurebayashi N, Murayama T (2008) Engineering a novel multifunctional green fluorescent protein tag for a wide variety of protein research. PLoS ONE **3**: e3822

Krebbers E, Herdies L, De Clercq A, Seurinck J, Leemans J, Van Damme J, Segura M, Gheysen G, Van Montagu M, Vandekerckhove J (1988) Determination of the processing sites of an Arabidopsis 2S albumin and characterization of the complete gene family. Plant Physiol **87**: 859–866

Krizek B (2009) *AINTEGUMENTA* and *AINTEGUMENTA-LIKE6* act redundantly to regulate Arabidopsis floral growth and patterning. Plant Physiol **150**: 1916–1929

Lee DW, Lee S, Oh YJ, Hwang I (2009) Multiple sequence motifs in the Rubisco small subunit transit peptide independently contribute to Toc159-dependent import of proteins into chloroplasts. Plant Physiol **151**: 129–141

Li H, Durbin R (2009) Fast and accurate short read alignment with Burrows-Wheeler transform. Bioinformatics **25**: 1754–1760

Ma H, McLean JR, Chao LFI, Mana-Capelli S, Paramasivam M, Hagstrom KA, Gould KL, McCollum D (2012) A highly efficient multifunctional tandem affinity purification approach applicable to diverse organisms. Mol Cell Proteomics **11**: 501–511

Mizukami Y, Fischer RL (2000) Plant organ size control: *AINTEGUMENTA* regulates growth and cell numbers during organogenesis. Proc Natl Acad Sci USA **97**: 942–947

Mohanty A, Luo A, DeBlasio S, Ling X, Yang Y, Tuthill DE, Williams KE, Hill D, Zadrozny T, Chan A, (2009) Advancing cell biology and functional genomics in maize using fluorescent protein-tagged lines. Plant Physiol **149**: 601–605

Morohashi K, Casas MI, Falcone Ferreyra ML, Falcone Ferreyra L, Mejía-Guerra MK, Pourcel L, Yilmaz A, Feller A, Carvalho B, Emiliani J, (2012) A genome-wide regulatory framework identifies maize pericarp color1 controlled genes. Plant Cell **24**: 2745–2764

Nelissen H, Rymen B, Coppens F, Dhondt S, Fiorani F, Beemster GTS (2013) Kinematic analysis of cell division in leaves of mono- and dicotyledonous species: a basis for understanding growth and developing refined molecular sampling strategies. Methods Mol Biol **959**: 247–264

Nelissen H, Eeckhout D, Demuynck K, Persiau G, Walton A, van Bel M, Vervoort M, Candaele J, De Block J, Aesaert S, (2015) Dynamic changes in ANGUSTIFOLIA3 complex composition reveal a growth regulatory mechanism in the maize leaf. Plant Cell **27**: 1605–1619

Nelson BK, Cai X, Nebenführ A (2007) A multicolored set of *in vivo* organelle markers for co-localization studies in Arabidopsis and other plants. Plant J **51**: 1126–1136

Omidbakhshfard MA, Proost S, Fujikura U, Mueller-Roeber B (2015) Growth-regulating factors (GRFs): a small transcription factor family with important functions in plant biology. Mol Plant **8**: 998–1010

Paramban RI, Bugos RC, Su WW (2004) Engineering green fluorescent protein as a dual functional tag. Biotechnol Bioeng **86**: 687–697

Proost S, Van Bel M, Vaneechoutte D, Van de Peer Y, Inzé D, Mueller-Roeber B, Vandepoele K (2015) PLAZA 3.0: an access point for plant comparative genomics. Nucleic Acids Res **43**: D974–D981

Quinlan AR, Hall IM (2010) BEDTools: a flexible suite of utilities for comparing genomic features. Bioinformatics **26**: 841–842

Rigaut G, Shevchenko A, Rutz B, Wilm M, Mann M, Séraphin B (1999) A generic protein purification method for protein complex characterization and proteome exploration. Nat Biotechnol **17**: 1030–1032

Rohila JS, Chen M, Chen S, Chen J, Cerny R, Dardick C, Canlas P, Xu X, Gribskov M, Kanrar S, (2006) Protein-protein interactions of tandem affinity purification-tagged protein kinases in rice. Plant J **46**: 1–13

Rubio V, Shen Y, Saijo Y, Liu Y, Gusmaroli G, Dinesh-Kumar SP, Deng XW (2005) An alternative tandem affinity purification strategy applied to Arabidopsis protein complex isolation. Plant J **41**: 767–778

Sarnowska E, Gratkowska DM, Sacharowski SP, Cwiek P, Tohge T, Fernie AR, Siedlecki JA, Koncz C, Sarnowski TJ (2016) The role of SWI/SNF chromatin remodeling complexes in hormone crosstalk. Trends Plant Sci **21**: 594–608

Schäffer U, Schlosser A, Müller KM, Schäfer A, Katava N, Baumeister R, Schulze E (2010) SnAvi: a new tandem tag for high-affinity protein-complex purification. Nucleic Acids Res **38**: e91

Schommer C, Debernardi JM, Bresso EG, Rodriguez RE, Palatnik JF (2014) Repression of cell proliferation by miR319-regulated TCP4. Mol Plant **7**: 1533–1544

Smaczniak C, Li N, Boeren S, America T, van Dongen W, Goerdayal SS, de Vries S, Angenent GC, Kaufmann K (2012) Proteomics-based identification of low-abundance signaling and regulatory protein complexes in native plant tissues. Nat Protoc **7**: 2144–2158

Thomas-Chollier M, Herrmann C, Defrance M, Sand O, Thieffry D, van Helden J (2012) RSAT peak-motifs: motif analysis in full-size ChIP-seq datasets. Nucleic Acids Res **40**: e31

Van Damme D, Coutuer S, De Rycke R, Bouget FY, Inzé D, Geelen D (2006) Somatic cytokinesis and pollen maturation in *Arabidopsis* depend on TPLATE, which has domains similar to coat proteins. Plant Cell **18**: 3502–3518

Van Leene J, Stals H, Eeckhout D, Persiau G, Van De Slijke E, Van Isterdael G, De Clercq A, Bonnet E, Laukens K, Remmerie N, (2007) A tandem affinity purification-based technology platform to study the cell cycle interactome in *Arabidopsis thaliana*. Mol Cell Proteomics **6**: 1226–1238

Van Leene J, Witters E, Inzé D, De Jaeger G (2008) Boosting tandem affinity purification of plant protein complexes. Trends Plant Sci **13**: 517–520

Van Leene J, Eeckhout D, Persiau G, Van De Slijke E, Geerinck J, Van Isterdael G, Witters E, De Jaeger G (2011) Isolation of transcription factor complexes from *Arabidopsis* cell suspension cultures by tandem affinity purification. Methods Mol Biol **754**: 195–218

Van Leene J, Eeckhout D, Cannoot B, De Winne N, Persiau G, Van De Slijke E, Vercruysse L, Dedecker M, Verkest A, Vandepoele K, (2015) An improved toolbox to unravel the plant cellular machinery by tandem affinity purification of *Arabidopsis* protein complexes. Nat Protoc **10**: 169–187

Van Leene J, Blomme J, Kulkarni SR, Cannoot B, De Winne N, Eeckhout D, Persiau G, Van De Slijke E, Vercruysse L, Vanden Bossche R, (2016) Functional characterization of the Arabidopsis transcription factor bZIP29 reveals its role in leaf and root development. J Exp Bot **67**: 5825–5840

Varagona MJ, Schmidt RJ, Raikhel NV (1992) Nuclear localization signal(s) required for nuclear targeting of the maize regulatory protein Opaque-2. Plant Cell **4**: 1213–1227

Vercruyssen L, Verkest A, Gonzalez N, Heyndrickx KS, Eeckhout D, Han SK, Jégu T, Archacki R, Van Leene J, Andriankaja M, (2014) ANGUSTIFOLIA3 binds to SWI/SNF chromatin remodeling complexes to regulate transcription during *Arabidopsis* leaf development. Plant Cell **26**: 210–229

Verkest A, Abeel T, Heyndrickx KS, Van Leene J, Lanz C, Van De Slijke E, De Winne N, Eeckhout D, Persiau G, Van Breusegem F, (2014) A generic tool for transcription factor target gene discovery in Arabidopsis cell suspension cultures based on tandem chromatin affinity purification. Plant Physiol **164**: 1122–1133

Wendrich JR, Boeren S, Möller BK, Weijers D, De Rybel B (2017) In vivo identification of plant protein complexes using IP-MS/MS. Methods Mol Biol **1497**: 147–158

White DWR (2017) PEAPOD limits developmental plasticity in Arabidopsis. bioRxiv102707

Wu Q, Luo A, Zadrozny T, Sylvester A, Jackson D (2013) Fluorescent protein marker lines in maize: generation and applications. Int J Dev Biol **57**: 535–543

Yilmaz A, Nishiyama MYJ Jr, Fuentes BG, Souza GM, Janies D, Gray J, Grotewold E (2009) GRASSIUS: a platform for comparative regulatory genomics across the grasses. Plant Physiol **149**: 171–180

Yun HY, Eipper BA (1995) Addition of an endoplasmic reticulum retention/retrieval signal does not block maturation of enzymatically active peptidylglycine α-amidating monooxygenase. J Biol Chem **270**: 15412–15416

Zhang D, Sun W, Singh R, Zheng Y, Cao Z, Li M, Lunde C, Hake S, Zhang Z (2018) GRF-interacting factor1 (gif1) regulates shoot architecture and meristem determinacy in maize. Plant Cell **30**: 360–374

Zhang Y, Liu T, Meyer CA, Eeckhoute J, Johnson DS, Bernstein BE, Nusbaum C, Myers RM, Brown M, Li W, (2008) Model-based analysis of ChIP-Seq (MACS). Genome Biol **9**: R137